AWARD NUMBER: W81XWH-17-1-0496

TITLE: Targeting B cell-mediated Type II Autoimmunity in Gastric Carcinogenesis

PRINCIPAL INVESTIGATOR: Mohamad El-Zaatari

CONTRACTING ORGANIZATION: Regents of the University of Michigan
Ann Arbor, MI 48109

REPORT DATE: August 2018

TYPE OF REPORT: Annual

PREPARED FOR: U.S. Army Medical Research and Materiel Command
Fort Detrick, Maryland 21702-5012

REPORT DOCUMENTATION PAGE

Form Approved
OMB No. 0704-0188

1. REPORT DATE	2. REPORT TYPE	3. DATES COVERED
August 2018	Annual	1 Aug 2017 – 31 Jul 2018

4. TITLE AND SUBTITLE
Targeting B cell-mediated Type II Autoimmunity in Gastric Carcinogenesis

5a. CONTRACT NUMBER

5b. GRANT NUMBER
W81XWH-17-1-0496

5c. PROGRAM ELEMENT NUMBER

6. AUTHOR(S)
Mohamad El-Zaatari

E-Mail: mohamade@med.umich.edu

5d. PROJECT NUMBER

5e. TASK NUMBER

5f. WORK UNIT NUMBER

7. PERFORMING ORGANIZATION NAME(S) AND ADDRESS(ES)

Regents of the University of Michigan
Ann Arbor, MI 48109

8. PERFORMING ORGANIZATION REPORT NUMBER

9. SPONSORING / MONITORING AGENCY NAME(S) AND ADDRESS(ES)

U.S. Army Medical Research and Materiel Command
Fort Detrick, Maryland 21702-5012

10. SPONSOR/MONITOR'S ACRONYM(S)

11. SPONSOR/MONITOR'S REPORT NUMBER(S)

12. DISTRIBUTION / AVAILABILITY STATEMENT

Approved for Public Release; Distribution Unlimited

13. SUPPLEMENTARY NOTES

14. ABSTRACT
The purpose of this project is to evaluate the contribution of gastric B cells to the development of gastric pre-neoplastic lesions in response to *Helicobacter* infection. The conclusion of the project will be a pre-clinical evaluation of utilizing rituximab (anti-CD20) to ameliorate gastric metaplastic lesions in this setting. The relevance to the military is due to deployment in areas with prevalent *Helicobacter pylori* (*H. pylori*) contamination, even in the drinking water in certain areas, which increase the risk to military personnel and veterans. Long-term *H. pylori* infection induces gastric pre-neoplastic lesions, which increase the risk of gastric cancer. If positive, the outcome will propose the use of rituximab to reduce the risk of carcinogenic development in military personnel exhibiting gastric metaplastic lesions due to ongoing or previous *H. pylori* infection.
The aims of years 1 and 2 are to ***(1)*** describe the specific nature of B cells in the *Helicobacter*-infected stomach (subtypes, functions and interaction with T cells), and ***(2)*** the downstream activities that contribute to disease. Year 3 will test the pre-clinical assay with rituximab.
Year 1 has successfully ***(i)*** set up the necessary mouse models and 6-month infections for year 2 analyses, and ***(ii)*** generated transcriptional heatmaps of gastric B cell subsets. These outcomes and progress will be described in the report in more detail.

15. SUBJECT TERMS
Helicobacter; B cells; metaplasia; pre-neoplasia; B2 cells; B1 cells; class-switch recombination; B cell-T cell interactions; CD16; autoimmune response; antigen-dependent cell-mediated cytotoxicity (ADCC); gastric cancer.

16. SECURITY CLASSIFICATION OF:			17. LIMITATION OF ABSTRACT	18. NUMBER OF PAGES	19a. NAME OF RESPONSIBLE PERSON
a. REPORT	b. ABSTRACT	c. THIS PAGE			USAMRMC
Unclassified	Unclassified	Unclassified	Unclassified		19b. TELEPHONE NUMBER *(include area code)*

Table of Contents

Page

1. **INTRODUCTION:** The purpose of this project is to evaluate the contribution of gastric B cells to the development of gastric pre-neoplastic lesions in response to *Helicobacter* infection. The conclusion of the project will be a pre-clinical evaluation of utilizing rituximab (anti-CD20) to ameliorate gastric metaplastic lesions in this setting. The relevance to the military is due to deployment in areas with prevalent *Helicobacter pylori* (*H. pylori*) contamination, even in the drinking water in certain areas, which increase the risk to military personnel and veterans. Long-term *H. pylori* infection induces gastric pre-neoplastic lesions, which increase the risk of gastric cancer. If positive, the outcome will propose the use of rituximab to reduce the risk of carcinogenic development in military personnel exhibiting gastric metaplastic lesions due to ongoing or previous *H. pylori* infection. The strategy encompasses ***1)*** describing the specific nature of B cells in the *Helicobacter*-infected stomach (subtypes, functions and interaction with T cells), ***2)*** the downstream activities that contribute to disease (pathological autoimmune responses that rely on B cell autoantibodies), and ***3)*** pre-clinical testing of rituximab (anti-CD20) that abolishes B cells, and assessing its ability to ameliorate gastric metaplastic lesions. Since the experiments require mouse breeding and 6-month long *Helicobacter* infections, the objective of year 1 was to establish mouse models and initiate infections that will be analyzed in year 2. However, year 1 still encompassed some characterization of gastric B cells that was performed and contributed to a journal publication as will be described later.

2. **KEYWORDS:** *Helicobacter*; B cells; metaplasia; pre-neoplasia; B2 cells; B1 cells; class-switch recombination; B cell-T cell interactions; CD16; autoimmune response; antigen-dependent cell-mediated cytotoxicity (ADCC); gastric cancer.

3. **ACCOMPLISHMENTS:** As described in the statement of work, the aim of year 1 was to develop mouse models and set up *Helicobacter* infections (that require 6 months) in preparation for year 2 analysis. Year 1 also included descriptive objectives for characterizing gastric B cells.

What were the major goals of the project? Within the scope of the overarching goal of the project described in the *Introduction* above, year 1 aimed to describe the nature of gastric B cells, and develop mouse models and set up infections for year 2 analyses. The tasks included:

i. Develop and infect a mouse model that will enable the evaluation of B cell-T cell interactions in the context of gastric metaplasia, to be analyzed in year 2 (SA1-Major Task 1: specified with an endpoint of year 2, months 3-5 on SOW).

ii. Develop a mouse model that will enable the infection and evaluation of B2 versus B1 contribution to gastric metaplasia, to be analyzed in year 2 (SA1-Major Task 2.1: specified with an endpoint of year 2, months 9-11 on SOW).

iii. Characterize B2 versus B1 cells in gastric metaplasia (SA1-Major Task 2.2: specified with an endpoint of year 1, months 8-10 on SOW).

iv. Generate and analyze a mouse model that will evaluate the contribution of class-switch recombination in B cells to gastric pathology, to be analyzed by the end of year 1 (SA1-Major Task 3: specified with an endpoint of year 1, months 8-12 on SOW).

v. Generate a mouse model that will enable the infection and evaluation of autoantibody-mediated gastric pathology, to be analyzed in year 2 (SA2-Major Task 1: specified with an endpoint of year 2, months 7-9 on SOW).

What was accomplished under these goals?

i. Develop and infect a mouse model that will enable the evaluation of B cell-T cell interactions in the context of gastric metaplasia, to be analyzed in year 2.

On the SOW, this is annotated as Specific Aim 1, Major Task 1. Generation of the mouse model is specified with an endpoint of Year 1 Months 3-8. The endpoint for infection and analysis is year 2 month 3.

The objective for this task for year 1 has been achieved. The $CD19^{cre}H2Ab1^{flox/flox}$ mouse model has been generated (**Fig. 1**) and is currently infected.

The experiment will compare metaplastic development in $CD19^{cre}H2Ab1^{flox/flox}$ lacking MHCII expression by B cells, relative to $H2Ab1^{flox/flox}$ controls that sustain MHCII expression by B cells. MHCII-lacking B cells are unable to undergo B cell-T cell interactions via MHCII-TCR.

ii. Develop a mouse model that will enable the infection and evaluation of B2 versus B1 contribution to gastric metaplasia in year 2.

On the SOW, this is annotated as Specific Aim 1, Major Task 2.1. The generation of $CD19^{Cre}PU.1^{flox/flox}$ model is scheduled for an endpoint of year 2 month 3. As such, the generation of this model is currently in progress.

The $CD19^{Cre}PU.1^{flox/flox}$ model develops an expansion of B1 cells at the expense of B2 cells. Hence the model will be used to differentiate the roles of B2 versus B1 cells in gastric metaplasia, by comparing $CD19^{Cre}PU.1^{flox/flox}$ versus $PU.1^{flox/flox}$ control littermates.

After generation, the $CD19^{Cre}PU.1^{flox/flox}$ will be infected for 6 months and analyzed.

As annotated on the SOW, the mouse generation is expected to be completed in year 2 as predicted.

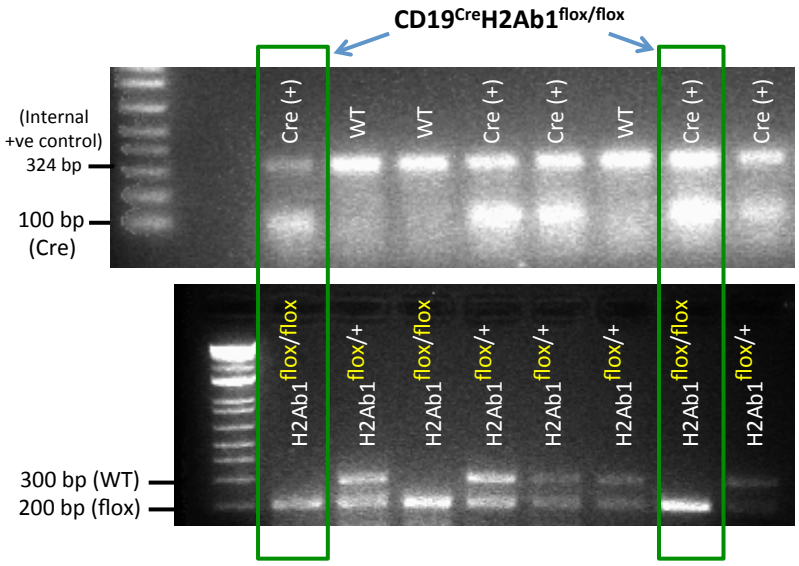

Figure 1. Generation of $CD19^{Cre}H2Ab1^{flox/flox}$ mice. RT-PCR of Cre (100bp, *top panel*) and H2Ab1-flox (200bp) versus WT (300bp) (*bottom panel*), which generated [CD19-Cre H2Ab1flox/flox] mice (green boxes).

iii. Characterize B2 versus B1 cells in gastric metaplasia.

On the SOW, this is annotated as Specific Aim 1, Major Task 2.2. The endpoint for these experiments is specified to be on Year 1, Month 10.

The objectives for this task have been completed, although the results deviated from expectation.

The markers for B1a cells are $CD43^+CD5^+$, while B1b cells are $CD43^+CD5^-$. The majority of gastric $B220^+$ B cells did not express B1 cell markers, i.e. they were negative for CD43 and CD5 (**Fig. 2, *Middle Panel, Bottom Flow Chart***; sub-gating $B220^+$ cells to CD43 and CD5). In contrast, B220-negative gastric cells did express CD43 and CD5 (**Fig. 2, *Middle Panel, Top Flow Chart***), but sub-gating to $CD43^+$ and/or $CD5^+$ positive cells showed they coincided with $CD11b^+Ly6G^+$ and $CD11b^+Ly6G^-$ myeloid cells (**Fig. 2, *Right Panel***). Therefore, the majority of gastric B cells ($B220^+$) are B2 cells during chronic *Helicobacter* infection.

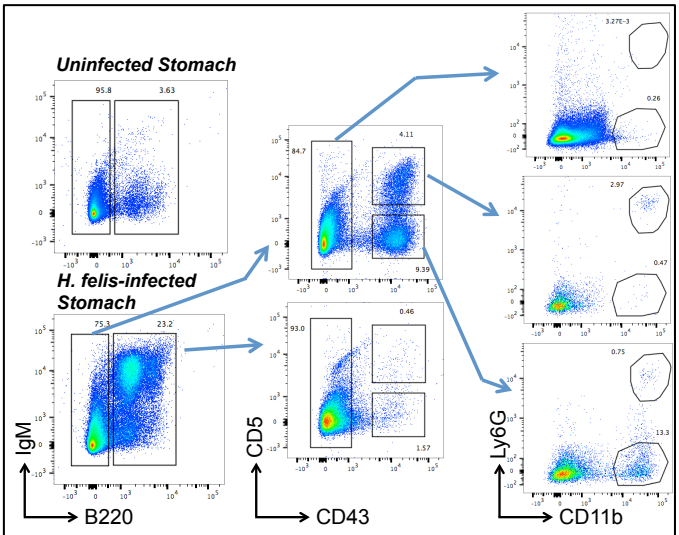

Figure 2. The majority of gastric B cells during *Helicobacter* infection are B2 cells. *Left Panel,* Flow Cytometric analysis of uninfected *versus H. felis*-infected stomachs showing an increase in $B220^+$ B cells. *Middle Panel,* sub-gating of gastric B220- versus B220+ cells shows that the majority of CD43+ and/or CD5+ cells are within the B220- population. *Right Panel*, gastric B220-CD43+CD5+/- populations overlap with CD11b+Ly6G- and CD11b+Ly6G+ myeloid cells.

Since we did not detect gastric B1 cells, we used this aim to transcriptionally profile different subsets of gastric B2 cells. We profiled $B220^+IgM^-$, $B220^+IgM^{low}$, and $B220^+IgM^{high}$ (**Fig. 3**). The transcriptional heatmap is presented in **Fig. 3**. As a validation for the results, $B220^+IgM^-$ expressed IGHG (but not IGHM) indicating class switching in this population (**Fig. 3**). In contrast, $B220^+IgM^+$ expressed IGHM (but not IGHG) indicating B cells that had not class-switched (**Fig. 3**). We did not detect transcriptional differences between $B220^+IgM^{low}$ and $B220^+IgM^{high}$. The analysis detected MHC-II expression in all B cell populations (**Fig. 3**), which are required for B cell-T cell interactions. Moreover, the analysis detected distinct expression patterns between class-switched versus non-class switched gastric B cells, which will be useful for future analyses of gastric B cell functions.

In conclusion, the gastric B cells are predominantly B2 cells and we have determined the transcriptional profiles of class-switched versus non-class-switched gastric B2 cells. This information will be utilized for future mechanistic investigation of gastric B cell functions.

iv. Generate and analyze a mouse model that will evaluate the contribution of class-switch recombination in B cells to gastric pathology, to be analyzed by the end of year 1.

On the SOW, this is annotated as Specific Aim 1, Major Task 3. The endpoint for these experiments is specified to be on year 1, month 12.

AID$^{-/-}$ mice fail to undergo B cell class-switch recombination, and these mice are therefore proposed for this sub-aim. These mice have been bred, are currently infected, and will be analyzed early in year 2. Unfortunately, due to the prolonged period required for breeding, we could not meet the timeline of completing the analyses by the end of year 1 for this sub-aim.

However, the 6-month infection period will be completed soon and the mice analyzed. Therefore, despite the delay, the overall results of the subaim are still expected to be obtained before the end of year 2 as projected in the SOW.

v. Generate a mouse model that will enable the infection and evaluation of autoantibody-mediated gastric pathology, to be analyzed in year 2.

On the SOW, this is annotated as Specific Aim 2. The endpoint for these experiments is specified to be on year 2, month 9.

This aim proposes the generation and use of the CD16$^{-/-}$ mouse model, which is incapable of undergoing antigen-dependent cell-mediated cytotoxicity (ADCC), which is required for autoantibody-mediated pathology. This aim will therefore assess the contribution of autoantibody-mediated pathology to gastric metaplastic lesions.

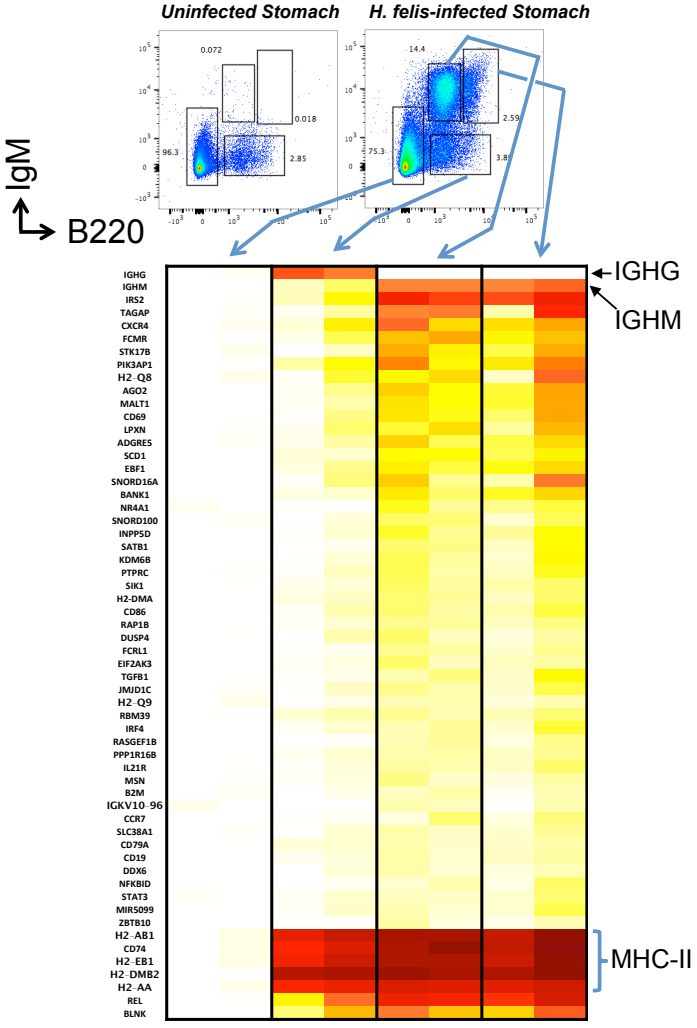

Figure 3. Transcriptional profiling of gastric B cell subsets. *Top Panel*, gastric B cell subsets. *Lower Panel*, transcriptional heatmaps between distinct gastric B cell populations. Each population is represented by cells isolated from 2 infected mouse stomachs (one column for each mouse).

The endpoint for year 1 of this aim has been achieved, and the CD16$^{-/-}$ mice are currently breeding in our facility, which meets the end point of this aim specified for year 1 on the SOW.

What opportunities for training and professional development has the project provided?

1) This grant contributed to a first-author publication by the PI in *Gastroenterology* 154(1):140-153 (2018), on the topic of this proposal (*the published paper is attached to the Appendix of this report*).

2) This grant supported the PI's attendance of the Digestive Disease Week (DDW) 2018 Conference. By enabling the PI to travel and attend this conference, this contributed to the PI moderating the cutting-edge Funderburg Symposium at DDW 2018, moderating another two scientific sessions, presenting one oral presentation, and interacting with other investigators studying gastric and GI carcinogenesis.

3) This grant's support for travel to DDW 2018 enabled the PI to attend the "AGA Grantee Networking Event", which included representatives and grant officers from both the DoD and the NIH. The meeting provided training on DoD and NIH grant applications.

4) This grant enabled the PI to attend a mock R01 study section at Case Western Reserve University, which trained the PI on the study section process. The meeting comprised a currently active NIH Scientific Review

Officer and previous members of an NIH study section. This training was carried out by the Midwest Digestive Disease Research Center (DDRC) alliance – an interdisciplinary alliance between digestive centers comprising University of Michigan, Mayo, University of Chicago, University of Cincinnati, Washington University and Case Western Reserve University.

How were the results disseminated to communities of interest?

Nothing to Report.

What do you plan to do during the next reporting period to accomplish the goals?

In the second year, the following will be determined:

1) The contribution of B cell-T cell interaction to gastric pathology by analyzing the infected $CD19^{cre}H2Ab1^{flox/flox}$ model versus $H2Ab1^{flox/flox}$ control.

2) The contribution of the B2 versus B1 cells to gastric pathology by analyzing the infected $CD19^{Cre}PU.1^{flox/flox}$ model versus $PU.1^{flox/flox}$ control.

3) The contribution of class-switch recombination to gastric pathology by analyzing the infected $AID^{-/-}$ model relative to WT control.

4) The contribution of autoantibody-mediated gastric pathology by preventing autoantibody interaction with target self cells using infected $CD16^{-/-}$ mice relative to WT.

Overall, these studies will determine the contribution of distinct aspects of gastric B cell function to gastric pathology, following chronic *Helicobacter* infection. The pre-clinical study evaluating Rituximab (anti-CD20) will then ensue in year 3.

4. **IMPACT:**

What was the impact on the development of the principal discipline(s) of the project?

The characterization of gastric B cells, which we performed, had not been performed previously. The gene expression heatmap of gastric B cell subsets enables better understanding of these cells, their differences, and will guide future mechanistic studies.

However, the impact for most of the experiments set up in year 1 will not be achieved until the analyses are complete in year 2. Such analyses will determine the contribution of distinct B cell functions to gastric pathology. This will be followed by a pre-clinical evaluation of anti-B cell therapy against gastric pre-cancerous lesions in year 3.

The overall impact will therefore determine the contribution of B cells to this disease, and assess the potential usefulness of B cell neutralizing antibodies in ameliorating outcomes. This will be a useful strategy to military personnel who had chronically been exposed to *Helicobacter* infection while on active duty.

What was the impact on other disciplines?

Better understanding of the immune cell environment in the stomach is critical for understanding gastric diseases in general and for the general public in addition to the military.

The proposal also develops the technical ability to isolate gastric immune cells from the stomach and construct their gene expression profiles.

What was the impact on technology transfer?

Nothing to Report.

What was the impact on society beyond science and technology?

Nothing to Report.

5. **CHANGES / PROBLEMS:**

Changes in approach and reasons for change

There are no significant changes to report. There was a variation on obtaining the transcriptional profiles of gastric B1 versus B2 cells. We did not observe gastric B1 cells to be detectable, but rather the majority to be in the B2 category. The change in approach therefore transcriptionally profiled the B2 subtypes instead of comparing B1 versus B2 expression profiles.

Actual or anticipated problems or delays and actions or plans to resolve them

There was a delay in analyzing the $AID^{-/-}$ mice (lack class-switching) because these mice required a longer breeding period than projected. However, they are now infected and will be analyzed before the end of year 2, which will meet the prediction for the final endpoint regarding this proposed sub-aim.

Changes that had a significant impact on expenditures

Nothing to Report.

Significant changes in use or care of human subjects, vertebrate animals, biohazard, and / or select agents

Nothing to Report.

Significant changes in use or care of human subjects

Nothing to Report.

Significant changes in use or care of vertebrate animals

Nothing to Report.

Significant changes in use of biohazards and/or select agents

Nothing to Report.

6. **PRODUCTS:**

Publications, conference papers, and presentations

Journal Publication: *(Paper Attached to **Appendix**)*

El-Zaatari M., Bass A.J., Bowlby R., Zhang M., Syu L.J., Yang Y., Grasberger H., Shreiner A., Tan B., Bishu S., Leung W.K., Todisco A., Kamada N., Cascalho M., Dlugosz A.A., and J.Y. Kao. Indoleamine 2,3-dioxygenase 1, Increased in Human Gastric Pre-Neoplasia, Promotes Inflammation and Metaplasia in Mice and is Associated with Type II Hypersensitivity/Autoimmunity. *Gastroenterology* 154(1):140-153 (2018).

Acknowledgement of federal support: Yes.

Website(s) or other Internet site(s)

Nothing to Report.

Technologies or techniques

Isolation of immune cell subtypes from inflamed gastric tissue and profiling their gene expression signatures. The protocol for this technique has been shared in the *Gastroenterology* publication listed above.

Inventions, patent applications, and/or licenses

Nothing to Report.

Other Products

Nothing to Report.

7. **PARTICIPANTS & OTHER COLLABORATING ORGANIZATIONS**

What individuals have worked on the project?

Name:	*Mohamad El-Zaatari*

Project Role:	*PI*
Researcher Identifier (e.g. ORCID ID):	0000-0002-1390-9489
Nearest person month worked:	*9*
Contribution to Project:	*Dr. El-Zaatari supervised experimental design, execution and interpretation of data.*
Funding Support:	*75% effort supported by the DoD PRCRP (remaining 25% by institutional support)*

Name:	*Min Zhang*
Project Role:	*Technician*
Researcher Identifier (e.g. ORCID ID):	N/A
Nearest person month worked:	*6*
Contribution to Project:	*Dr. Zhang assisted Dr. El-Zaatari with the execution of the experiments.*
Funding Support:	*50% effort supported by the DoD PRCRP (remaining 50% by other grant awards and institutional support)*

Has there been a change in the active other support of the PD/PI(s) or senior/key personnel since the last reporting period?

Nothing to Report.

What other organizations were involved as partners?

Nothing to Report.

8. **SPECIAL REPORTING REQUIREMENTS**

Nothing to Report.

9. **APPENDICES:**

Attached on page 10.

Gastroenterology 2018;154:140–153

Indoleamine 2,3-Dioxygenase 1, Increased in Human Gastric Pre-Neoplasia, Promotes Inflammation and Metaplasia in Mice and Is Associated With Type II Hypersensitivity/Autoimmunity

Mohamad El-Zaatari,[1] Adam J. Bass,[2] Reanne Bowlby,[3] Min Zhang,[1] Li-Jyun Syu,[4] Yitian Yang,[1] Helmut Grasberger,[1] Andrew Shreiner,[1] Bei Tan,[1] Shrinivas Bishu,[1] Wai K. Leung,[5] Andrea Todisco,[1] Nobuhiko Kamada,[1] Marilia Cascalho,[6] Andrzej A. Dlugosz,[4] and John Y. Kao[1]

[1]Department of Internal Medicine-Gastroenterology, University of Michigan, Ann Arbor, Michigan; [2]Department of Medical Oncology and the Center for Cancer Genome Discovery, Dana-Farber Cancer Institute, Boston, Massachusetts; [3]Canada's Michael Smith Genome Sciences Centre, British Columbia Cancer Agency, Vancouver, British Columbia, Canada; [4]Department of Dermatology, School of Medicine, University of Michigan, Ann Arbor, Michigan; [5]Department of Medicine, University of Hong Kong, Queen Mary Hospital, Hong Kong, China; and [6]Department of Surgery, University of Michigan, Ann Arbor, Michigan

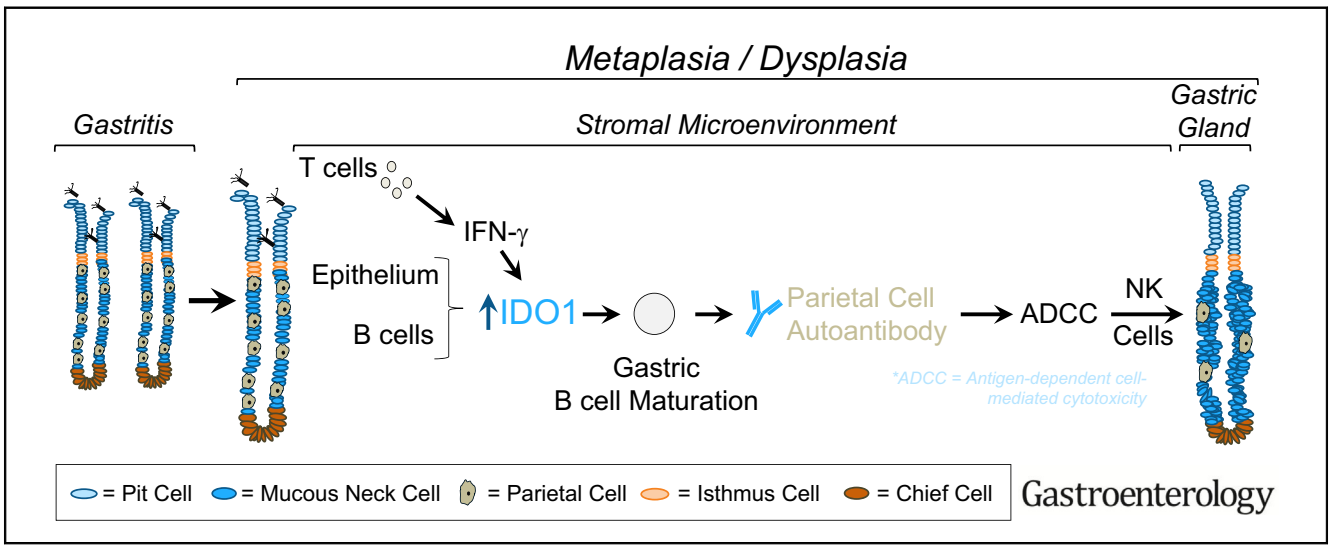

BACKGROUND & AIMS: Chronic gastrointestinal inflammation increases the risk of cancer by mechanisms that are not well understood. Indoleamine-2,3-dioxygenase 1 (IDO1) is a heme-binding enzyme that regulates the immune response via catabolization and regulation of tryptophan availability for immune cell uptake. IDO1 expression is increased during the transition from chronic inflammation to gastric metaplasia. We investigated whether IDO1 contributes to the inflammatory response that mediates loss of parietal cells leading to metaplasia. **METHODS:** Chronic gastric inflammation was induced in *Ido1*$^{-/-}$ and CB57BL/6 (control) mice by gavage with *Helicobacter felis* or overexpression of interferon gamma in gastric parietal cells. We also performed studies in *Jh*$^{-/-}$ mice, which are devoid of B cells. Gastric tissues were collected and analyzed by flow cytometry, immunostaining, and real-time quantitative polymerase chain reaction. Plasma samples were analyzed by enzyme-linked immunosorbent assay. Gastric tissues were obtained from 20 patients with gastric metaplasia and 20 patients without gastric metaplasia (controls) and analyzed by real-time quantitative polymerase chain reaction; gastric tissue arrays were analyzed by immunohistochemistry. We collected genetic information on gastric cancers from The Cancer Genome Atlas database. **RESULTS:** *H felis* gavage induced significantly lower levels of pseudopyloric metaplasia in *Ido1*$^{-/-}$ mice, which had lower frequencies of gastric B cells, than in control mice. Blood plasma from *H felis*–infected control mice had increased levels of autoantibodies against parietal cells, compared to uninfected control mice, but this increase was lower in *Ido1*$^{-/-}$ mice. Chronically inflamed stomachs of *Ido1*$^{-/-}$ mice had significantly lower frequencies of natural killer cells in contact with parietal cells, compared with stomachs of control mice. *Jh*$^{-/-}$ mice had lower levels of pseudopyloric metaplasia than control mice in response to *H felis* infection. Human gastric pre-neoplasia and carcinoma specimens had increased levels of *IDO1* messenger RNA compared with control gastric tissues, and IDO1 protein colocalized with B cells. Co-clustering of *IDO1* messenger RNA with B-cell markers was corroborated by The Cancer Genome Atlas database. **CONCLUSIONS:** IDO1 mediates gastric metaplasia by regulating the B-cell compartment. This process appears to be

EDITOR'S NOTES

BACKGROUND AND CONTEXT

Chronic gastric inflammation predisposes an individual to gastric pre-cancerous lesions, but the mechanisms in which immune cells regulate gastric carcinogenesis are not understood.

NEW FINDINGS

The immunomodulatory molecule indoleamine-2,3-dioxygenase 1 (IDO1) mediates gastric pre-neoplastic development by regulating the B cell compartment, via a mechanism that exhibited association with gastric autoimmunity.

LIMITATIONS

This study did not prove that autoimmunity is a central mechanism underlying the development of gastric pre-neoplastic lesions, although associations with autoimmunity were presented.

IMPACT

The study presents new evidence that the B cell compartment – regulated by IDO1 – is a necessary component in gastric pre-neoplastic development, and warrants further investigation of autoimmunity in gastric carcinogenesis.

associated with type II hypersensitivity/autoimmunity. The role of autoimmunity in the progression of pseudopyloric metaplasia warrants further investigation.

Keywords: Kynurenine; Gastritis; SPEM; Humoral Immunity.

It is well established that a prolonged latency period of chronic inflammation (~8–10 years) precedes the development of gastrointestinal cancers,[1,2] including gastric cancer.[3,4] Therefore, the quality of inflammation can change during this long-lived process; in the later stages of chronic inflammation, immune cells should display a pathologic phenotype that can trigger carcinogenesis. This "switch" in the inflammatory milieu has not been characterized. We have recently identified a mouse model (the $Gli1^{-/-}$ model) in which the progression from chronic gastric inflammation to metaplasia does not occur.[5] This model led to the identification of several metaplasia-associated genes, several of which played a role in immunity. One of these differentially induced genes was indoleamine-2,3-dioxygenase 1 (IDO1). We therefore sought to assess the contribution of IDO1 to gastric metaplasia and determine its mechanism.

IDO1 is traditionally known to suppress T-cell immunity.[6] It functions by metabolizing tryptophan into kynurenine.[7] In doing so, this enzyme restricts the tryptophan pool in tumor microenvironments, therefore reducing T-cell numbers.[6] The enzyme also increases kynurenine levels in the microenvironment, which stimulates regulatory T-cell (Treg) differentiation.[8] However, recently, IDO1 has been described to regulate other populations, for example, B cells[9–11] and epithelial cells.[12] In addition, we recently reported that IDO1 regulates neutrophil abundance (rather than T cells) and their interferon (IFN)-γ production during cecal *Clostridium difficile* infection.[13] Hence, IDO1 function is likely variable within different pathologic contexts.

Given the role of IDO1 in immunity and its association with gastric metaplasia, we sought to determine its function and mechanism in this disease. We hypothesized that IDO1 is a critical component involved in the transition from chronic inflammation to gastric metaplasia. The elucidation of IDO1 function would therefore shed some light on the immune components involved in this transition. To address this hypothesis, we analyzed chronically inflamed gastric microenvironments in IDO1-deficient vs proficient mice, and compared our findings to molecular pathways of human gastric cancer.

Methods

Human Gastric Samples

Human gastric samples were obtained during surgical procedures according to standard tissue procurement mechanisms managed by the Department of Pathology of the University of Hong Kong, under Institutional Review Board–approved protocol number UW-140611. The samples were de-identified and private information, such as names, dates of birth, or medical record numbers, was not provided. The samples were collected from the lesser gastric curvature of patients with intestinal metaplasia vs normal patients. The increase in marker expression (*TFF-2* and *CD44*) indicating spasmolytic peptide-expressing metaplasia was confirmed in the metaplastic samples. A total of 20 normal and 20 metaplastic gastric samples were used. For paraffin immunohistochemistry of human gastric tissue, a tissue microarray of human inflamed, cancerous, and normal stomach was used (US Biomax, Rockville, MD; cat. #IC00011c).

Animals

$Ido1^{-/-}$ and CB57BL/6 (generated by Baban et al[14]) were obtained from The Jackson Laboratory (Bar Harbor, ME) stock #005867. $Jh^{-/-}$ mice on a C57BL/6 background were provided by Dr Cascalho (University of Michigan).[15] All the animals used in our studies were male, except for Supplementary Figure 13, in which both males and females were used for the analysis. All animal models used in this study including wild-type (WT), $Ido1^{-/-}$, *IFN-γ*, *IFN-γ-Ido1*$^{-/-}$, and $Jh^{-/-}$ were on a CB57BL/6 background. Animals were housed in groups (3–5 animals per cage) in micro-isolator cages under specific pathogen-free conditions. Animals were infected at 8 weeks of age for 6 months. Before infection, cage bedding was replaced between cages repetitively for 14 days to normalize the microflora

Abbreviations used in this paper: **EBV, Epstein-Barr virus; FACS, fluorescence-activated cell sorting; IDO1, indoleamine-2,3-dioxygenase-1; IFN, interferon; MDSC, myeloid-derived suppressor cell; mRNA, messenger RNA; NK, natural killer; PE, phycoerythrin; RT-qPCR, real-time quantitative polymerase chain reaction; TCGA, The Cancer Genome Atlas; Treg, regulatory T cell; WT, wild-type.**

Most current article

0016-5085/$36.00
https://doi.org/10.1053/j.gastro.2017.09.002

between cages. The H^+/K^+-*ATPase-IFN-γ* model was provided by Dr Dlugosz (University of Michigan).[16]

Fluorescence-Activated Cell Analysis and Sorting

Fluorescence-activated cell sorting (FACS) was performed as described previously.[13] Live cells were gated using LIVE/DEAD Fixable Aqua Dead Cell Stain Kit (cat. #L34957; Life Technologies, Grand Island, NY). The following antibodies were used for B cells: B220-phycoerythrin [PE]-Cy7 (clone RA3-6B2, cat. #103221; Biolegend, San Diego, CA), and IgM-PE (clone eB121-15F9, cat. #12-5890-81, eBiosciences, San Diego, CA). The following antibodies were used for T cells and myeloid cells: CD4-fluorescein isothiocyanate (clone GK1.5, cat. #11-0041-85; eBioscience, San Diego, CA), CD25−PE−Cy7 (clone PC61.5, cat. #25-0251-81; eBioscience), CD11b−eFluor

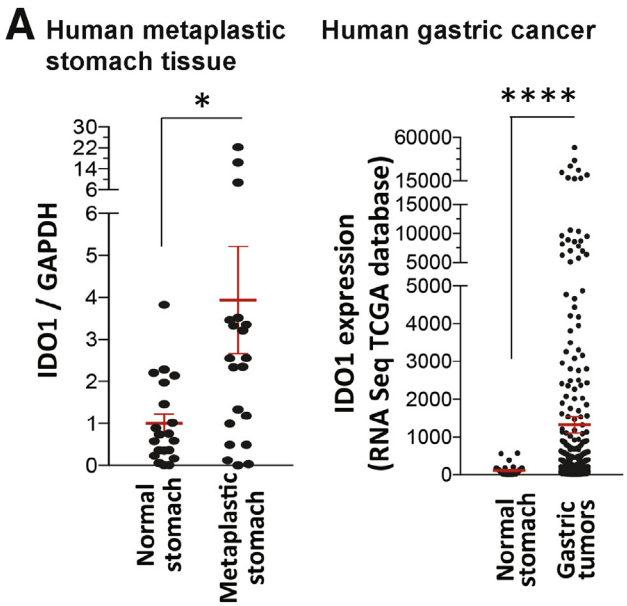

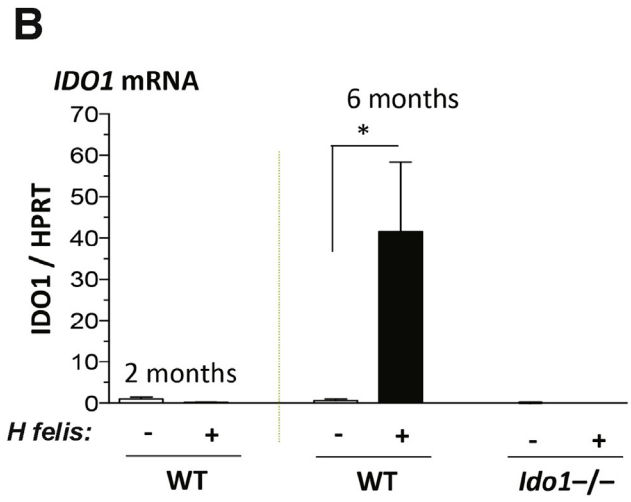

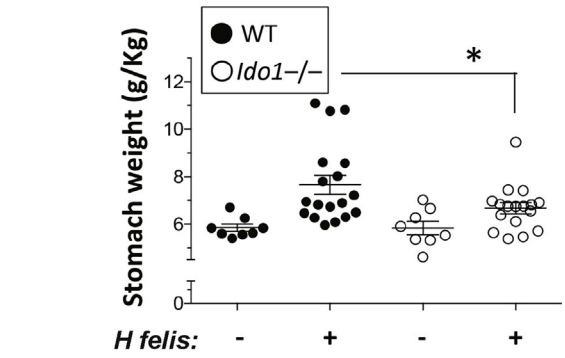

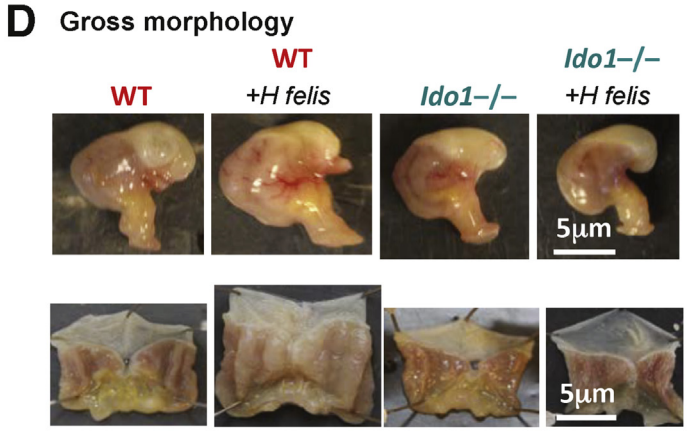

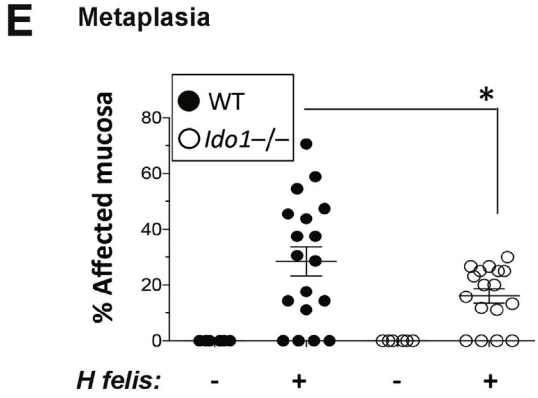

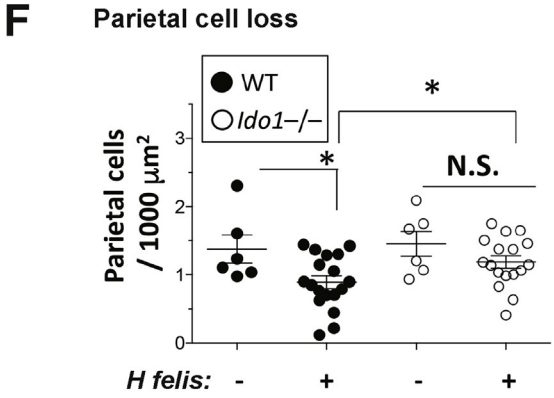

450 (clone M1/70, cat. #48-0112-82; eBioscience), and Ly6G-PE (clone 1A8, cat. #127607; BioLegend, San Diego, CA). RNA extraction of isolated cells for microarray analysis was performed using the RNEasy Microkit (Qiagen, Valencia, CA).

Statistics

Data were tested for normality using the Shapiro–Wilk W test (Prism, GraphPad Software, La Jolla, CA). Data were compared using 1-way analysis of variance with Dunnet's (parametric) or Dunn's (nonparametric) multiple comparison tests (Prism). P values $<.05$ were considered significant.

Study Approval

All studies were approved by the University of Michigan Institutional Animal Care and Use Committee (PRO00005890). The human data were obtained by analyzing de-identified samples collected during surgical procedures performed by the Department of Pathology of the University of Hong Kong, under IRB-approved protocol number UW-140611. The Cancer Genome Atlas (TCGA) human data were obtained by analyzing de-identified databases generated previously by the TCGA study,[17] which did not require additional human sample collection.[17] Hence, IRB approval for the TCGA data was described in the previous study for which the samples were originally collected.[17] The human tissue array was obtained from US Biomax and had been previously de-identified by the company.

Further information about the Methods utilized in this article can be accessed in the Supplementary Material.

Results

Indoleamine-2,3-Dioxygenase 1 Contributes to Gastric Metaplasia

We identified *IDO1* messenger RNA (mRNA) to be induced in human gastric metaplastic tissue relative to normal (Figure 1*A*, *left panel*, and Supplementary Figure 1). Moreover, using TCGA database, *IDO1* mRNA was also induced in gastric cancers relative to normal stomach (Figure 1*A*, *right panel*). To model the role of IDO1 in gastric immunopathology, we chronically infected WT and *Ido1*$^{-/-}$ mice with *Helicobacter felis*. We previously established that gastric metaplasia develops at 6 months, but not at 2 months, after *H felis* infection.[5] Consistent with this previous observation,[5] we found *IDO1* mRNA to be induced at 6 months, but not 2 months, after *H felis* infection (Figure 1*B*). The induction of gastric *IDO1* mRNA was abrogated in *Ido1*$^{-/-}$ mice (Figure 1*B*). As IDO1 metabolizes tryptophan into kynurenine (Supplementary Figure 2*A*), we confirmed the levels of kynurenine to be induced in the chronically infected stomach, which was abolished in the *Ido1*$^{-/-}$ mice (Supplementary Figure 2*B*). The generation of downstream metabolites of kynurenine was not substantial in the inflamed stomach (Supplementary Figure 2*B*). These experiments confirmed the induction of *IDO1* mRNA and stimulation of IDO1 activity during chronic (6 months) *H felis* infection, which was abrogated in *Ido1*$^{-/-}$ mice.

We then investigated the role of IDO1 in the generation of gastric metaplasia. As stomach hypertrophy, assessed by measuring stomach weight, is directly associated with metaplasia,[5] we measured the stomach weight normalized to total body weight of the mouse. We observed an increase in relative stomach weight in 6-month *H felis*–infected WT mice relative to uninfected WT mice (Figure 1*C*). However, this increase was significantly reduced in *Ido1*$^{-/-}$ mice (Figure 1*C*). This is corroborated by the macroscopic appearance of the stomachs in WT vs *Ido1*$^{-/-}$ mice (Figure 1*D*). The reduction in stomach weight increase of infected *Ido1*$^{-/-}$ mice correlated with a significant reduction in metaplastic lesions (Figure 1*E*; quantification criteria in Supplementary Figure 3*A*). Hence *Ido1*$^{-/-}$ mice exhibited a significant reduction of gastric metaplastic lesions.

Because parietal cell loss triggers metaplastic development,[18] we assessed the degree of parietal cell loss in the *Ido1*$^{-/-}$ mice by staining for H^+/K^+-ATPase-β as shown in Supplementary Figure 3*B*. While infected WT mice showed a significant reduction in parietal cell number (per area), this significant reduction was not observed in *Ido1*$^{-/-}$ stomachs (Figure 1*F*). We conclude that IDO1 contributes to the development of parietal cell loss and gastric metaplasia.

Indoleamine-2,3-Dioxygenase 1 Regulates B-Cell Abundance During Chronic Gastric Inflammation

To investigate the mechanism of IDO1 in gastric inflammation, we used a mouse model that overexpresses IFN-γ in the stomach (H^+/K^+-*ATPase-IFN-*γ; will be referred to as *IFN-*γ model from here onward).[16] IFN-γ is a known inducer of IDO1,[19] and this model exhibited a robust induction of *IDO1* mRNA in the stomach (Supplementary Figure 4*A*). We have previously shown the *IFN-*γ mouse

Figure 1. IDO1 deletion reduces gastric hypertrophy, metaplastic lesions, and parietal cell loss. (*A*) *Left panel:* RT-qPCR of *IDO1* mRNA expression (relative to *GAPDH*) in human gastric metaplasia samples relative to normal stomach. *Right panel: IDO1* mRNA expression levels by RNASeq in gastric tumor vs normal stomach tissue obtained from TCGA. Each *dot* represents tissue from 1 patient. (*B*) RT-qPCR analysis of *IDO1* mRNA in 2 months and 6 months *H felis*–infected WT stomachs vs uninfected, and 6 months *H felis*–infected *Ido1*$^{-/-}$ stomachs vs uninfected. (*C*) Stomach weight normalized to total body weight in WT vs *Ido1*$^{-/-}$ mice ± 6-month *H felis* infection. (*D*) Representative images showing the gross morphologic appearance of WT vs *Ido1*$^{-/-}$ mouse stomachs ± *H felis*. (*E*) *Scatterplot* showing the percentage area of metaplastic gastric mucosa in WT vs *Ido1*$^{-/-}$ mice ± 6-month *H felis*. Metaplasia was assessed and quantified using trefoil factor 2 (TFF-2) and intrinsic factor (IF) as shown in Supplementary Figure 3*A*. (*F*) *Scatterplot* showing the number of parietal cells per 1000 μm^2 of glandular tissue in WT vs *Ido1*$^{-/-}$ mice ± 6-month *H felis*. Parietal cells were quantified using Fiji (ImageJ) and the fluorescent staining described in Supplementary Figure 3*B*. n = 5 mice per uninfected group, 18 mice in the infected WT group, and 17 mice in the infected *Ido1*$^{-/-}$ group. Error bars represent the mean and SEM. Data were compared using 1-way analysis of variance with Dunnet's (parametric) or Dunn's (nonparametric) for multiple comparison tests (Prism), and unpaired *t* test (parametric) or Mann–Whitney test (nonparametric) for single comparisons (Prism). Each data point represents 1 mouse. *$P < .05$; **$P < .01$; ****$P < .0001$. NS, not significant.

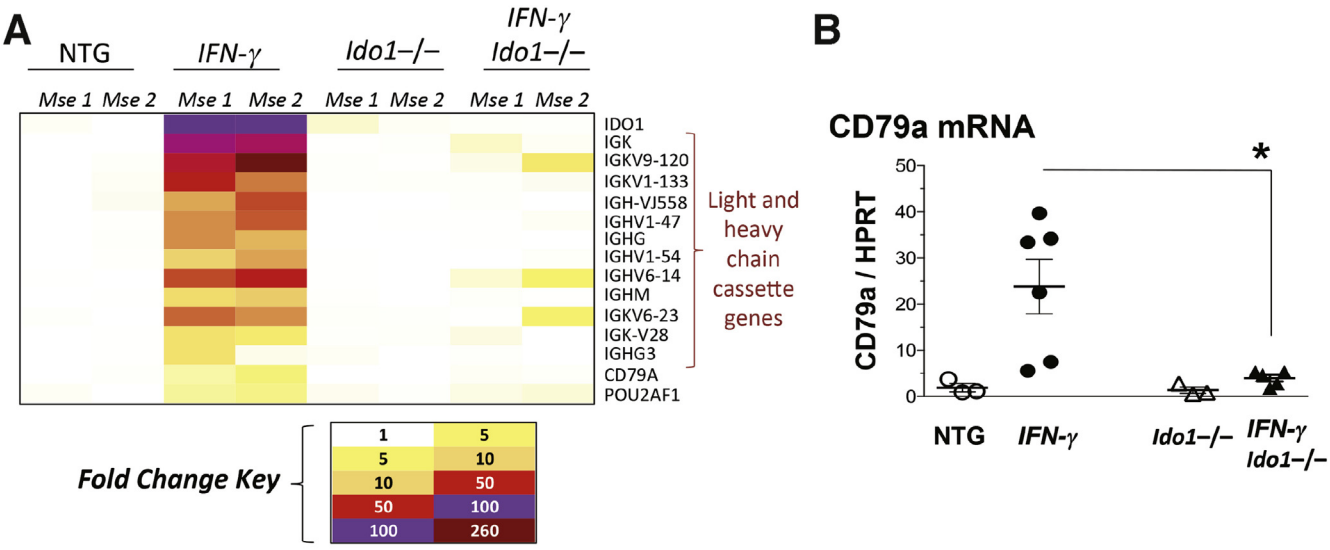
A
NTG
IFN-γ
Ido1−/−
IFN-γ Ido1−/−
Mse 1 Mse 2 Mse 1 Mse 2 Mse 1 Mse 2 Mse 1 Mse 2
IDO1
IGK
IGKV9-120
IGKV1-133
IGH-VJ558
IGHV1-47
IGHG
IGHV1-54
IGHV6-14
IGHM
IGKV6-23
IGK-V28
IGHG3
CD79A
POU2AF1
Light and heavy chain cassette genes
Fold Change Key
1 5
5 10
10 50
50 100
100 260
B
CD79a mRNA
CD79a / HPRT
NTG
IFN-γ
Ido1−/−
IFN-γ Ido1−/−

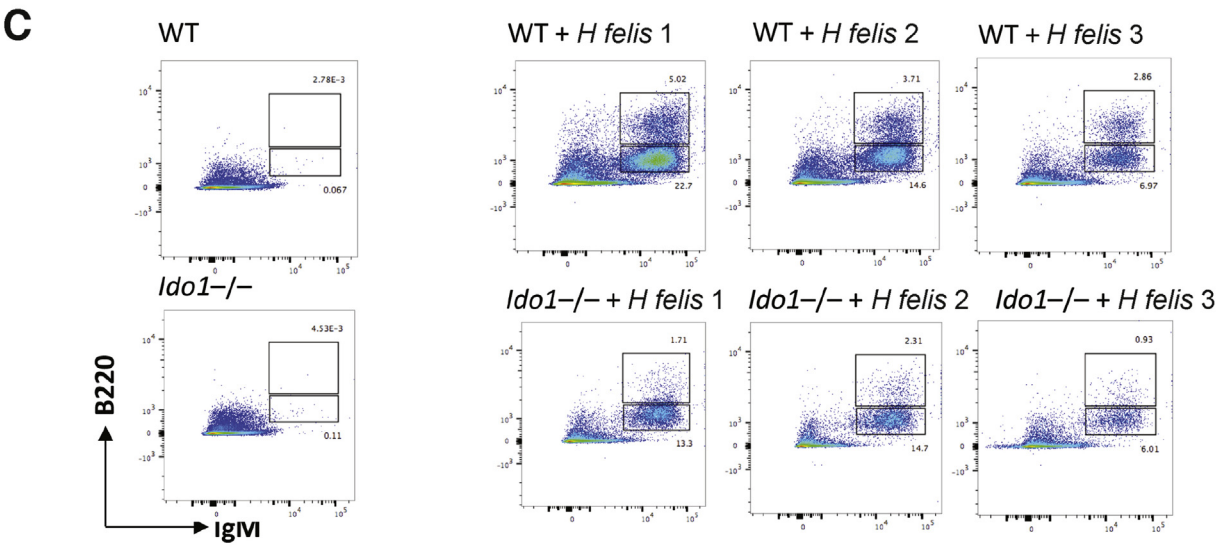
C
WT
WT + H felis 1
WT + H felis 2
WT + H felis 3
Ido1−/−
Ido1−/− + H felis 1
Ido1−/− + H felis 2
Ido1−/− + H felis 3
B220
IgM

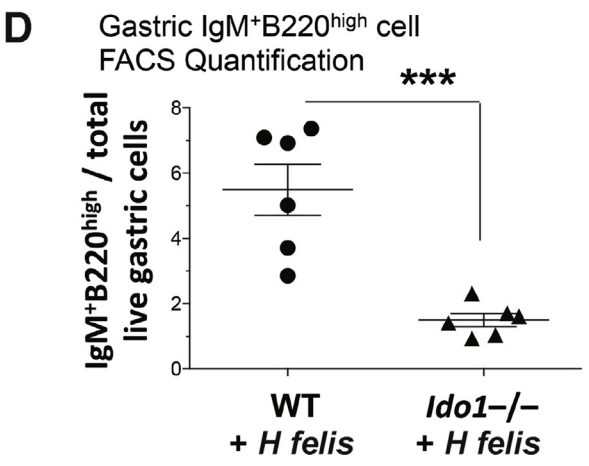
D
Gastric IgM+B220high cell FACS Quantification
IgM+B220high / total live gastric cells
WT + H felis
Ido1−/− + H felis

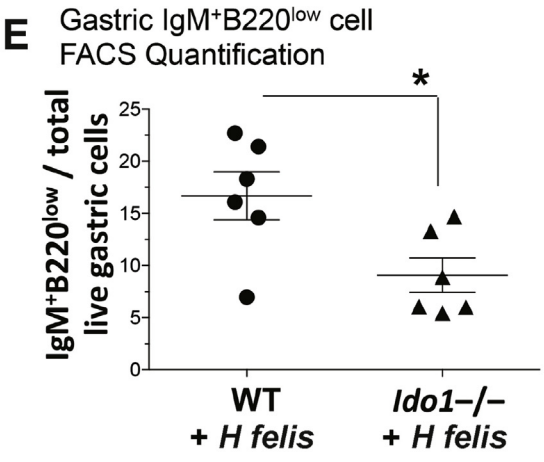
E
Gastric IgM+B220low cell FACS Quantification
IgM+B220low / total live gastric cells
WT + H felis
Ido1−/− + H felis

model to develop chronic gastric inflammation. To study the function of IDO1, we bred the *IFN-γ* model onto an IDO1-deficient background to generate *H*$^{+}$/*K*$^{+}$*-ATPase-IFN-γ/Ido1*$^{-/-}$ (will be referred to as *IFN-γ-Ido1*$^{-/-}$). The *IFN-γ-Ido1*$^{-/-}$ model lacked gastric *IDO1* expression and induction (Supplementary Figure 4*A*). We performed microarray analysis to determine the effect of IDO1 loss. The microarray showed that the IDO1-dependent genes in the inflamed stomach almost exclusively comprised immunoglobulin light and heavy chain cassettes, *CD79A*, and *Pou2af1*, which are B-cell markers (Figure 2*A*). These genes were up-regulated in the *IFN-γ* model vs nontransgenic, but were not induced in *IFN-γ-Ido1*$^{-/-}$ (Figure 2*A*). The expression patterns of *CD79A*, *IDO1*, and *Igkv1-133* from this array were confirmed by real-time quantitative polymerase chain reaction (RT-qPCR) (Figure 2*B* and Supplementary Figure 4). This indicated that IDO1 deficiency was affecting the B-cell compartment in the inflamed gastric mucosa.

To investigate the effect of IDO1 deficiency on B cells, we performed B-cell FACS analysis in *Ido1*$^{-/-}$ vs WT *H felis*–infected stomachs. We used the classification from previous studies, which characterized immature naïve B cells as B220^{low}IgM^{+} and mature naïve B cells as B220^{high}IgM^{+}.[20,21] We observed a robust increase in both immature and mature naïve gastric B-cell populations during chronic *H felis* infection (Figure 2*C*). However, there was a significant decrease in mature B220^{high}IgM^{+} and immature B220^{low}IgM^{+} B cells in infected *Ido1*$^{-/-}$ stomachs (Figure 2*C*–*E*). This indicated that mature naïve B cells were either depleted in inflamed *Ido1*$^{-/-}$ stomachs or otherwise exhibited an increased rate of class switch recombination. To determine the mechanism, we assessed class switch recombination of B cells in chronically inflamed *Ido1*$^{-/-}$ vs WT stomachs.

Our identification of class-switched B cells began with the observation of the expression of immunoglobulin-γ heavy-chain and variable κ light-chain cassettes (Supplementary Figure 5*A*). We used a B-cell–deficient model lacking the joining chain (*Jh*$^{-/-}$ mice) and observed the effect of B-cell deficiency on the expression of heavy- and light-chain cassettes (Supplementary Figure 5*A*, *left panel*). *H felis* infection (6 months) increased the expression of *Ighm*, *Ighg*, *Igl*, and *Igk* genes (for μ heavy chain, γ heavy chain, λ light chain, and κ light chain, respectively), which were abolished in the infected *Jh*$^{-/-}$ stomachs (Supplementary Figure 5*A*, *left panel*). However, the majority of these cassette genes, except for *Ighm* (μ) and Iglv (λ variable), were not expressed by B220^{+}IgM^{+} B cells (Supplementary Figure 5*A*, *middle panel*). Instead, they were expressed by CD11b^{-}Ly6G^{+} immune cells (Supplementary Figure 5*A*, *right panel*). Analysis of these CD11b^{-}Ly6G^{+} immune cells, after being negatively gated for CD4^{-}CD8^{-}, showed that they coincided with B220^{+}IgM^{-} B cells (Supplementary Figure 5*B*–*H*). These data correlated with a previous report showing that "class-switched B cells" expressed the B220^{+}IgM^{low} markers (as opposed to B220^{+}IgM^{high} for naïve B cells).[22] Moreover, these CD11b^{-}Ly6G^{+} immune cells expressed the *Ly6c* gene (Supplementary Figure 5*A*, *right panel, third gene from the top*). This also correlated with a previous study that showed that *Ly6c* is a marker of a differentiation of B cells into plasma cells.[23] We therefore conclude that the CD11b^{-}Ly6G^{+} population (after negatively gating T cells) represents the class switched population producing IgG (*Ighg* gene). To determine the effect of IDO1, we measured the frequency of this CD11b^{-}Ly6G^{+} population, and showed that it was reduced, rather than increased, in chronically infected *Ido1*$^{-/-}$ stomachs (Supplementary Figure 5*I*). This demonstrated that the reduction of naïve B-cell population in inflamed *Ido1*$^{-/-}$ stomachs (Figure 2*C*) was not due to an increase in class switch recombination of these cells.

Indoleamine-2,3-Dioxygenase 1 Does Not Regulate Gastric CD4^{+} *T-Cell, Myeloid, or Myeloid-Derived Suppressor Cell Abundance*

IDO1 has traditionally been defined as an enzyme that metabolizes tryptophan into kynurenine.[7] In doing so, the enzyme diminishes the tryptophan pool required for T-cell proliferation[6] and generates kynurenine that stimulates Treg differentiation.[8] We therefore measured the abundance of CD4^{+} T cells and CD4^{+}CD25^{+} Tregs in infected WT and *Ido1*$^{-/-}$ stomachs. We first observed a clear increase in T-cell and Treg numbers after 6-month *H felis* infection (Supplementary Figure 6*A*). However, contrary to the commonly described role of IDO1, we did not observe a difference in CD4^{+} T-cell and CD4^{+}CD25^{+} Treg numbers between infected WT and *Ido1*$^{-/-}$ stomachs (Supplementary Figure 6*A*–*C*). In addition to the lack of difference in CD4^{+} T-cell numbers, we did not observe a significant difference in T-helper 1 cytokine expression (IFN-γ, tumor necrosis factor–α, and interleukin 1β) between WT and *Ido1*$^{-/-}$ stomach tissue (Supplementary Figure 6*D*). We conclude that *Ido1*$^{-/-}$ did not alter the T-cell response in the context of chronic gastric inflammation.

Because a recent study showed that IDO1 indirectly regulates myeloid-derived suppressor cell (MDSC) recruitment,[24] we quantified myeloid cells and MDSCs in the gastric microenvironment of WT and *Ido1*$^{-/-}$ stomachs. We observed a robust increase in gastric MDSCs after 6 months of *H felis* infection, but no difference was observed between infected WT

Figure 2. *Ido1*$^{-/-}$ stomachs display a B-cell–deficient phenotype. (*A*) Fold change heatmap of the differentially regulated genes induced in 2-month-old *IFN-gamma* but not in *IFN-gamma-Ido1*$^{-/-}$ stomachs. (*B*) RT-qPCR of the B-cell marker, *CD79a*, in *IFN-gamma* vs *IFN-gamma-Ido1*$^{-/-}$ stomachs (2 months old), relative to nontransgenic controls. (*C*) FACS analysis of immature naïve (IgM^{+}B220^{low}) and mature naïve (IgM^{+}B220^{high}) B cells in WT vs *Ido1*$^{-/-}$ stomachs ± *H felis* after 6-month infection. (*D*) Graphical representation of FACS mature naïve (IgM^{+}B220^{high}) B-cell percentages in *H felis*–infected WT vs *Ido1*$^{-/-}$ stomachs. (*E*) Graphical representation of FACS immature naïve (IgM^{+}B220^{low}) B-cell percentages in *H felis*–infected WT vs *Ido1*$^{-/-}$ stomachs. Error bars represent the SEM. Each data point represents 1 mouse. *$P < .05$; ***$P < .001$.

and *Ido1*$^{-/-}$ stomachs (Supplementary Figure 7*A*–*C*). We conclude that IDO1 does not regulate MDSC or myeloid cell frequency in the chronically inflamed stomach.

Indoleamine-2,3-Dioxygenase 1 Does Not Affect Helicobacter felis *Bacterial DNA Abundance*

H felis flagellar filament B (*Fla-B*) is used as an indicator of bacterial abundance.[5,25] Even though *Ido1*$^{-/-}$ showed a trend for increased *H felis* DNA in gastric tissue (which correlates with reduced gastric immunopathology), the difference in *H felis* DNA was not significant between WT and *Ido1*$^{-/-}$ (Supplementary Figure 8). This indicated that IDO1 did not have a significant effect on *H felis* bacterial abundance.

Indoleamine-2,3-Dioxygenase 1 Deficiency Correlates With Reduced Anti-Parietal Cell Autoantibody Levels and Natural Killer Cell-to-Cell Contact With Parietal Cells

The reduction of gastric B cells in *Ido1*$^{-/-}$ suggested that IDO1 might regulate the autoimmune response against parietal cells in the inflamed stomach. The presence of parietal cell autoantibody is a common occurrence in *Helicobacter pylori*–infected patients,[26] although the pathologic mechanism for these autoantibodies is not clear.[27] Autoimmune reactions, although responding to internal "self" antigen—as opposed to external antigen in the case of hypersensitivity—are believed to share overlapping mechanisms with hypersensitivity reactions.[28] There are 4 types of hypersensitivity reactions according to the Coombs and Gell classification.[29] Among the 4 types, only type II is dependent on antibody-mediated binding of target cells.[29] The latter mechanism can be mediated by antigen-dependent cell-mediated cytotoxicity, in which natural killer (NK) cells bind antibody-coated target cells and initiate cell death.[29] We therefore investigated whether hallmarks of type II hypersensitivity/autoimmunity were present and regulated by IDO1. In the following paragraph, we will only use the term *type II autoimmunity* as it involves the targeting of internal/"self" (parietal cell) antigen, rather than external antigen. We therefore assayed 2 hallmarks of type II autoimmunity: autoantibody binding to parietal cells and NK cell association with parietal cells.

We first measured anti-parietal cell autoantibody in infected WT vs *Ido1*$^{-/-}$ mouse plasma. While chronic *H felis* infection significantly increased anti-parietal cell antibodies measured by enzyme-linked immunosorbent assay, *Ido1*$^{-/-}$ mice did not exhibit such a robust significant increase (Figure 3*A*). We observed a significant increase of NK cell/parietal cell contact points in the chronically infected WT gastric mucosa, but not in the *Ido1*$^{-/-}$ gastric mucosa (Figure 3*B*–*D*). Low-power images and the negative control are also shown in Supplementary Figure 9. The latter images additionally suggest that the total number of NK cells might have been reduced in the infected *Ido1*$^{-/-}$ stomach (Supplementary Figure 9). Hence, the reduction in NK/parietal contact might have also been attributed to lower abundance of NK cells. Irrespective of either scenario, the data provide supportive evidence that the hallmarks of type II autoimmunity (parietal cell autoantibody and NK/parietal cell interaction) were reduced in inflamed *Ido1*$^{-/-}$ stomachs. Hence, a reduction of hallmarks of type II autoimmunity is associated with IDO1 deficiency in the chronically inflamed stomach.

Indoleamine-2,3-Dioxygenase 1 Alters the Transcriptional Profile of Gastric B Cells

To investigate the mechanism of how IDO1 regulates B cells, we first determined the expression pattern of IDO1. IDO1 was expressed by both gastric epithelial cells and B cells in metaplastic mouse stomach (Supplementary Figure 10*A*) and inflamed human stomach (Supplementary Figure 10*B*). Moreover, both stromal and epithelial expression of IDO1 was detected in human gastric cancer (Supplementary Figure 10*C*). Because B cells expressed IDO1 endogenously, we determined the effect of IDO1 deficiency on gastric B cells' transcriptional profile. We FACS sorted B cells from 6-month infected WT vs *Ido1*$^{-/-}$ gastric mucosa and performed microarray analysis (Figure 4). First, the microarray corroborated the enrichment of B-cell–specific genes in these isolated cells (Supplementary Figure 11 and Supplementary Dataset 1; for raw data, please refer to Supplementary Dataset 2). Second, the microarray identified differences in the transcriptional profile between WT and *Ido1*$^{-/-}$ gastric B cells (Figure 4 and Supplementary Dataset 3). Although the majority of the identified genes have not been characterized previously in B-cell function, the microarray still identified some known markers (Figure 4). These included the up-regulation of BMP receptor 2 (*Bmpr2*) in gastric *Ido1*$^{-/-}$ B cells. *Bmpr2* is not normally detected in WT gastric B cells after chronic infection with *H felis* (Figure 4), but is induced in IDO1-deficient gastric B cells (Figure 4). BMP signaling can play a role in modulating B-cell activation in certain contexts, such as bone marrow and peripheral blood, in which BMP signaling can repress B-cell proliferation[30–32] and antibody production[33]; the up-regulation of granzyme B (*Gzmb*) in gastric *Ido1*$^{-/-}$ B cells. *Gzmb* up-regulation is indicative of incomplete T-cell help[34]; and down-regulation of *VH11* (*Igh-V11*) in *Ido1*$^{-/-}$ gastric B cells. *VH11* is a marker of an autoreactive subset of B1 cells[35] (Figure 4). We did not observe an effect of IDO1 on the expression of maturation factors *Prdm1* (*Blimp1*), *Xbp-1*, *Bcl6*, or *Pax5* in gastric B cells (data not shown). Hence, although the mechanism of IDO1 regulation of B cells remains unclear, the data demonstrate an altered transcriptional profile—indicative of altered functionality—of *Ido1*$^{-/-}$ gastric B cells relative to WT.

B Cells Are Necessary for Metaplastic Development

Because a previous study showed that the cμ gene knockout of the constant immunoglobulin heavy chain locus (μMT mice) did not affect gastric metaplastic development,[36] we aimed to address this inconsistency. Several studies have shown that the μMT model does not

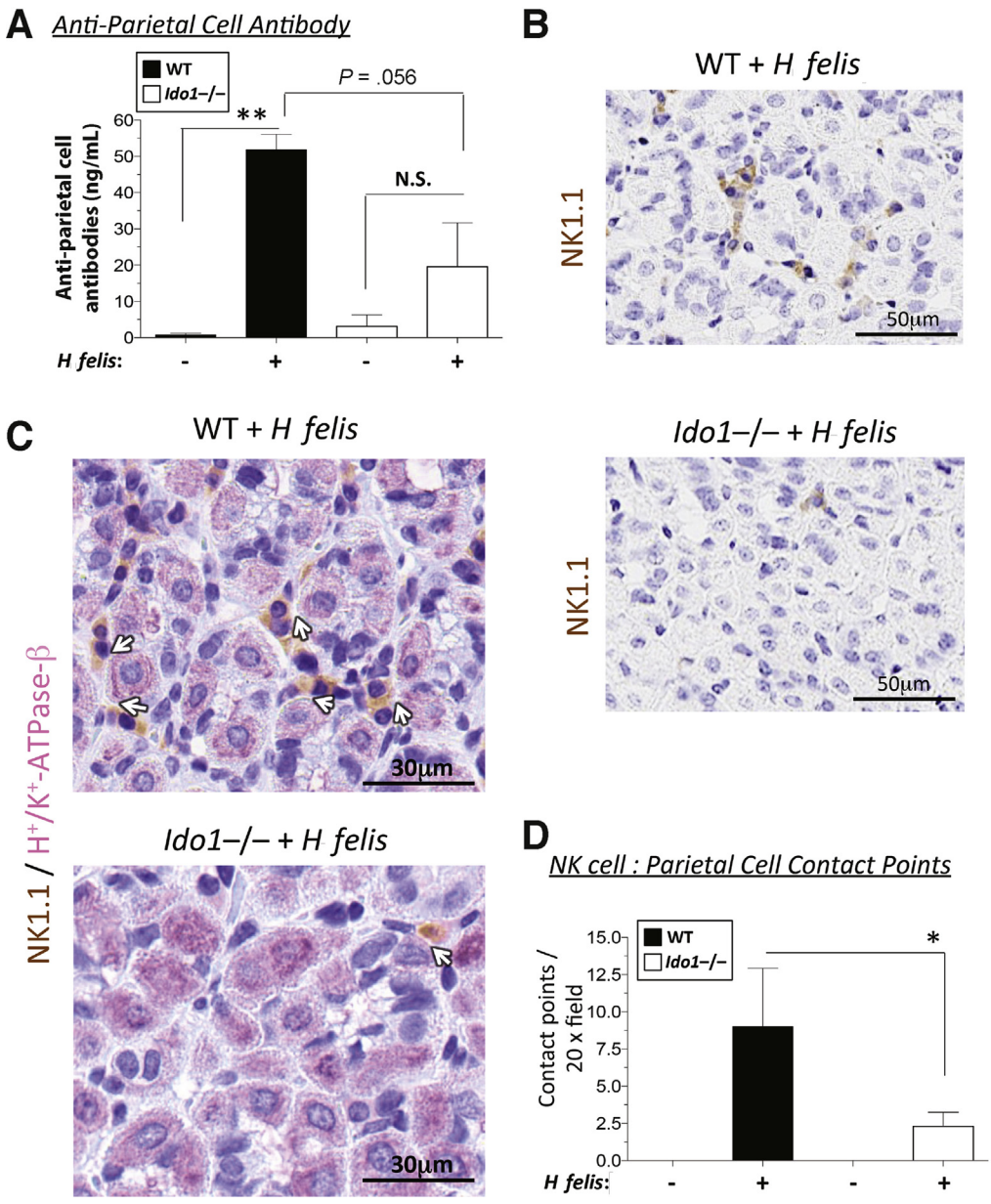

Figure 3. IDO1 deficiency is associated with reduced autoantibody production and NK cell-to-cell contact with parietal cells. (*A*) *Bar graph* representation of plasma anti-parietal cell antibody levels in 6-month infected WT vs *Ido1*$^{-/-}$ mice compared to uninfected controls. (*B*) Immunohistochemical staining of NK1.1-HRP antibody (*brown*) in 6-month infected WT vs *Ido1*$^{-/-}$ stomachs. These *insets* are obtained from the low-power images shown in Supplementary Figure 9*A*. (*C*) Immunohistochemical double staining of NK1.1-HRP (*brown*) and H^+/K^+-ATPase-β (*pink*) of parietal cells in 6-month infected WT vs *Ido1*$^{-/-}$ stomachs. *White arrows* indicate the contact points between the NK cells and the parietal cells. (*D*) *Bar graph* representation of morphometric quantification of NK cell/parietal cell contact points per 20× microscopic field. Data were compared using 1-way analysis of variance with Dunnet's (parametric) or Dunn's (non-parametric) for multiple comparison tests (Prism). Error bars represent the SEM. *$P < .05$; **$P < .01$.

exhibit total B-cell deficiency and, in fact, is capable of producing antibodies.[37–40] This is not surprising because heavy-chain genes are normally deleted from the chromosome during B cell class switching. Hence other downstream genes (eg, δ, γ, ε, or α) can be similarly utilized when the μ gene is genetically deleted in the μMT model. To avoid this redundancy, we used the *Jh*$^{-/-}$ mouse model,[41] which contains a disrupted J segment gene, and therefore exhibits complete B-cell and immunoglobulin deficiency.[38] While the chronically infected WT mice showed an expanded gastric $B220^+IgM^+$ B-cell populations compared to uninfected WT, the *Jh*$^{-/-}$ mice lost their gastric B cells (Figure 5*A* and quantification in Figure 5*B*). These mice did not exhibit a significant change in *H felis Fla-B* bacterial DNA (Supplementary Figure 12*A*). The loss of B cells was validated by RT-qPCR for *CD79a* and *Igk v1-133* (Supplementary Figure 12*B* and *C*). These *Jh*$^{-/-}$ mice exhibited significantly reduced metaplastic lesions in the stomach (Figure 5*C* and *D*). Hence, the data suggest that B cells contribute to metaplasia, contrary to the previous interpretation based on the μMT model.[36]

Indoleamine-2,3-Dioxygenase 1 and B Cell Markers Are Among the Highest-Regulated Genes That Cluster With a Human Gastric Adenocarcinoma Subtype

To correlate our finding to human gastric cancer, we used TCGA[17] to determine whether IDO1 and B-cell regulation are involved. *IDO1* and 5 B-cell markers (*IDO1*, *CD79A*, *IGHG1*, *IGLL5*, *IGHC*, and *IGVK-A2*) were among the 10 highest differentially induced gene, and clustered with 1

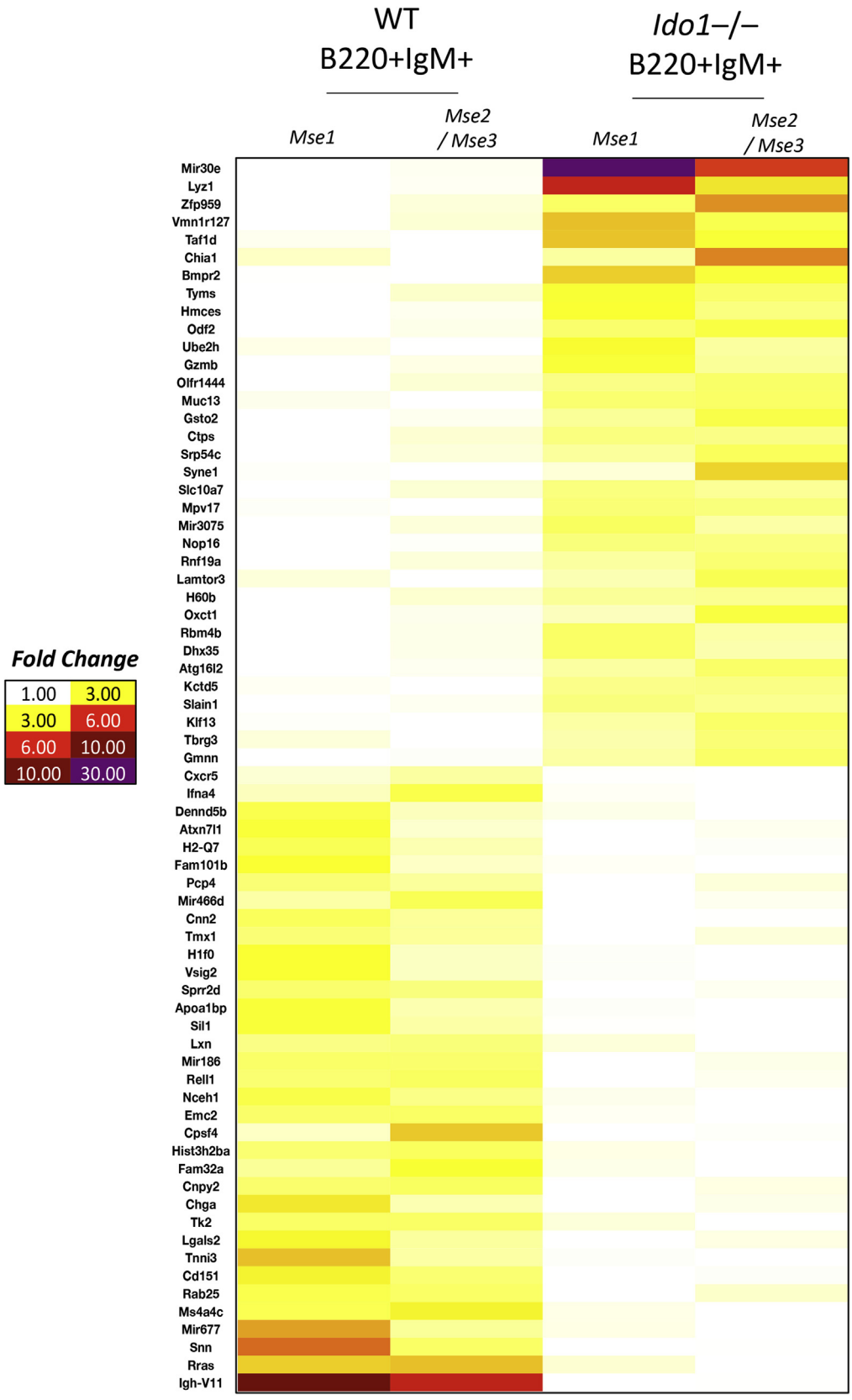

Figure 4. IDO1-deficient gastric B cells exhibit an altered transcriptional profile. Microarray heatmap of FACS-isolated gastric $B220^{+}IgM^{+}$ B cells from 6-month infected WT vs *Ido1* $^{-/-}$ stomachs. The microarray illustrates the altered transcription profile of *Ido1* $^{-/-}$ vs WT gastric B cells isolated from 6-month infected stomachs. "Mse 1" refers to isolated RNA from gastric B cells of 1 mouse, whereas "Mse 2/Mse 3" represents pooled isolated RNA from gastric B cells of 2 mice to serve as a replicate.

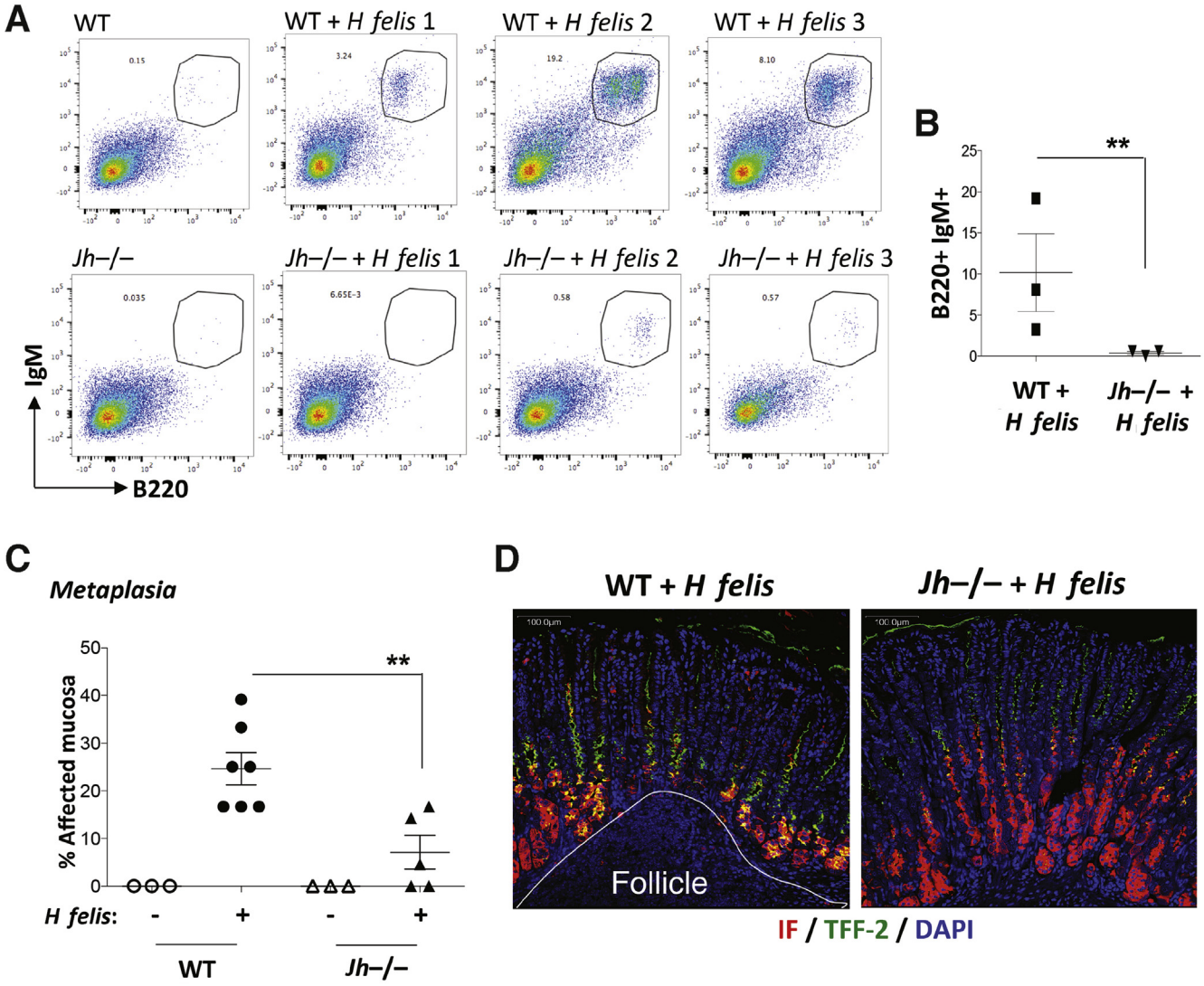

Figure 5. Mice with B-cell deficiency (lacking the JH locus) show reduced metaplasia. (*A*) FACS analysis of mature B220^{+}IgM^{+} B cells in 6-month *H felis*–infected WT vs *Jh*$^{-/-}$ stomachs. (*B*) Graphical representation of FACS percentages of B cells in *H felis*–infected WT vs *Jh*$^{-/-}$ stomachs. (*C*) Scatterplot showing the percentage of metaplastic gastric areas in WT vs *Jh*$^{-/-}$ mice ± 6-month *H felis*. (*D*) Representative images of metaplastic vs non-metaplastic areas from *H felis*–infected WT vs *Jh*$^{-/-}$ stomachs, respectively. Intrinsic factor (IF) = *red*; Trefoil factor 2 (TFF-2) = *green*; 4′,6-diamidino-2-phenylindole (DAPI) = *blue*. Error bars represent the SEM. Each data point represents 1 mouse. $^{**}P < .01$.

molecular subtype of human gastric adenocarcinoma called "expression cluster 2"[17] (Figure 6). The high expression of these markers in expression cluster 2 does not preclude the induction of IDO1 in other gastric cancer subtypes, as induction is generally detected in pooled gastric cancer samples in Figure 1*A*. However, as expression cluster 2 is associated with Epstein-Barr virus (EBV) infection,[17] this implicates stronger induction of *IDO1*/B cell signaling in heightened inflammatory immunopathology caused by EBV.

Mouse Models of Gastric Pre-Neoplasia Exhibit Some Similarity in Gene Induction Patterns to Human Expression Cluster 2

Because mouse models of gastric metaplasia are limited in that they fail to progress to gastric cancer, it was important to assess the relevance of our mouse studies to human cancer. Even though the pre-neoplastic models do no replicate the pathology of fully developed gastric cancer, we evaluated the suitability of our analyses by comparing gene expression patterns that were induced in both mouse models and human cancer subtypes from the TCGA.[17] We observed considerable overlap between the expression profiles corresponding to the *H felis* model and human expression cluster 2 (Supplementary Figure 13). *IDO1* was the highest-expressed common gene in these 2 sets (Supplementary Figure 13). Other commonly induced genes in cluster 2 included B-cell–specific genes, *CD79a*, *IgJ*, and *Pou2af1*, and the NK cell gene *NKG7* (Supplementary Figure 13). A similar result was obtained using the IFN-γ–overexpressing model, with highest similarity to expression cluster 2 (Supplementary Figure 14*A*). These

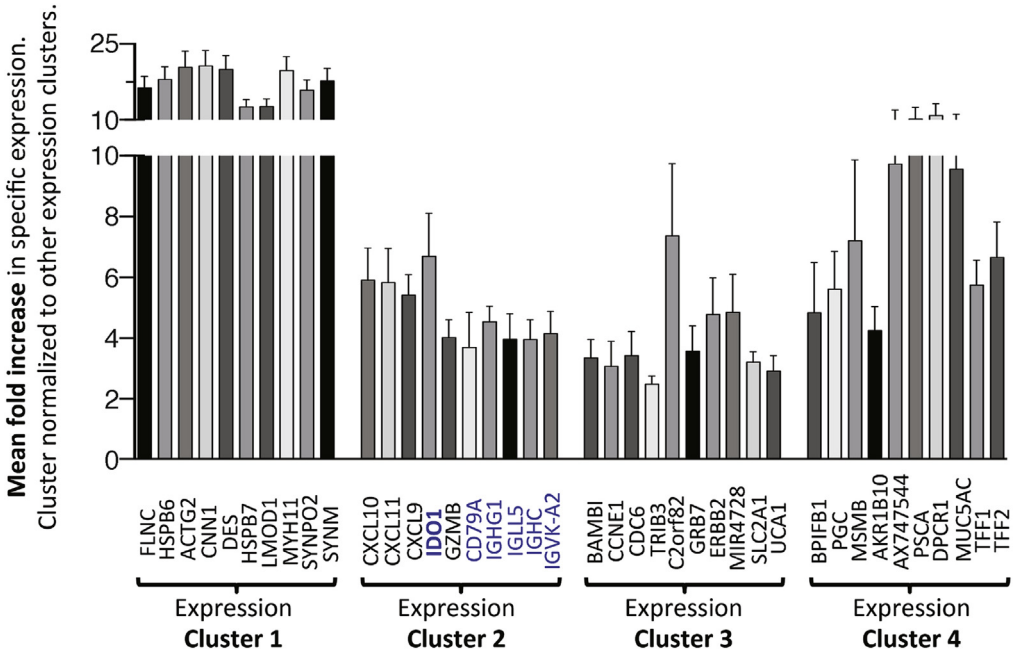

Figure 6. List of the top cluster-specific genes for each human expression cluster. *Bar graph* showing the top 10 most up-regulated genes in each expression cluster defined by TCGA study.[17] *IDO1* and B-cell–specific genes (*CD79A*, *IGHG1*, *IGLL5*, *IGHC*, and *IGVK-A2*) are highlighted in *blue font*. For each gene, the values represent the mean fold change in expression across the samples in that cluster. Error bars = mean ± SEM.

comparisons were also performed against the general TCGA classification of gastric cancer subtypes (ie, EBV, microsatellite instability, genomically stable, and chromosomal instability), and showed the highest similarity between the mouse pre-neoplastic models and the EBV subtype (Supplementary Figure 14*B* and *C*). This is not surprising because expression cluster 2 is enriched with EBV-positive cancers.[17] Therefore, some similarity exists in the patterns of differentially induced genes between mouse models of gastric pre-neoplasia and human adenocarcinoma.

Discussion

The major conclusion of this study is that IDO1 contributes to pseudopyloric metaplasia in the stomach. The mechanism appears to be mediated by IDO1 regulation of the B-cell compartment, which associates with hallmarks of type II autoimmunity. Our proposed mechanism is summarized in Graphical Abstract. This conclusion is based on the following experimental evidence. First, we showed that IDO1-deficient mice develop reduced metaplasia and gastric B-cell frequency. The effect on B cells was not due to increased class switching. In addition, no apparent impact on T-cell or myeloid cell abundance was detected. Second, we showed that this phenotype associates with a reduced autoantibody response against parietal cells, and reduced NK cell-to-cell contact with parietal cells, both of which represent hallmarks of reduced type II autoimmunity. Third, we showed that IDO1-deficient gastric B cells exhibit an altered transcriptional profile from WT gastric B cells, and that B cell-deficient mice develop reduced metaplastic lesions. Finally, we showed that the *IDO1* expression is strongly increased in human gastric metaplasia and cancer, and associates with B cell markers. Collectively, this experimental evidence suggests that IDO1-mediated B cell regulation contributes to pseudopyloric metaplasia, and associates with hallmarks of type II autoimmunity during gastric carcinogenesis.

Previous studies have shown associations between parietal cell autoantibodies, *H pylori* infection, and human gastric cancer,[42–48] although the pathologic mechanisms for these autoantibodies remain unclear. IDO1 has also been shown to be associated with human gastric cancer.[17,49,50] First, Strong et al[49] detected high IDO1 induction in EBV-associated gastric cancer.[49] Second, this was recently confirmed by an independent patient sample of EBV-associated gastric cancer.[50] Third, TCGA identified *IDO1* in 1 of the 4 types of patient expression clusters, called "expression cluster 2," which was associated with EBV-positive gastric cancer.[17] In this study, we showed that the *H felis* and IFN-γ–overexpressing mouse models were similar in their expression patterns to human expression cluster 2 and the EBV subtype. The similar induction of *IDO1* in EBV and *H felis* is possibly a manifestation of the heightened immune response and immunopathology in both infectious contexts. Furthermore, we also showed an induction of *IDO1* expression in human gastric metaplasia. Hence, the modeled pathways showed relevance to the gastric pre-neoplastic and neoplastic microenvironment. However, despite these observations, further work is required to determine the differences in the applicability of these mechanisms to human gastric pre-neoplastic etiology vs cancer.

One consideration in this study is that, despite our previous finding that IFN-γ overexpression sufficiently induces metaplasia,[16] we did not observe a difference in IFN-γ expression between infected WT and $Ido1^{-/-}$ stomachs. This observation is not surprising because IFN-γ functions upstream of *IDO1* induction, and inflamed $Ido1^{-/-}$ stomachs do not exhibit a difference in $CD4^{+}$ T-cell frequency. Thus,

we proposed that IDO1 functions downstream of IFN-γ, which is illustrated in Graphical Abstract.

The finding that IDO1 did not alter T-cell numbers or cytokine expression is not entirely surprising, given the recent findings by Thaker et al[12] in colorectal tumor models. In that study, the authors showed IDO1 deficiency to reduce colorectal polyps in the azoxymethane/dextran sodium sulfate model.[12] This parallels our finding that IDO1 deficiency reduces pre-neoplastic lesions in the stomach. However, their study also demonstrated that the reduction of polyps did not appear to be mediated by a T-cell mechanism.[12] However, they proposed IDO1 to act directly on neoplastic epithelial cell proliferation via β-catenin.[12] Another study showed—in line with our findings—that IDO1 is necessary for B-cell and autoantibody production in rheumatoid arthritis.[51] This contrasts with a recent study that reported that B-cell–intrinsic IDO1 suppresses T-cell–independent humoral immunity.[10] The difference between our study and the latter study is perhaps not surprising because *H felis*–mediated immunopathology requires T-cell–dependent adaptive immunity and B-cell-T-cell interactions,[36] whereas the latter study focused on thymic-independent B-cell activation.[10] However, our results shed new light on B-cell–mediated gastric metaplasia development, which is contrary to a previous report using the μMT model.[36] This is because the μMT model is not fully B-cell–deficient, as it is capable of producing antibodies and generating viable B cells.[37–40] Hence, it is clear from this study, and from our previous work in which IDO1 restricts neutrophil infiltration,[13] that the IDO1 mechanism is not limited to the traditionally described pathway of restricting T-cell proliferation. Moreover, the effect of IDO1 on B cells might also be subject to variability due to the heterogeneity of B-cell biology. This could depend on the extent of involvement of thymic-dependent vs independent responses, or B2 vs B1 contribution to the pathologic context under study. Future studies will explore these aspects as outlined in the following paragraph.

It is a novel and paradigm-shifting concept to consider B-cell involvement and autoreactive antigen-dependent cell-mediated cytotoxicity in gastric carcinogenesis. However, our observations are not surprising because the development of lymphoid follicles, which contain B-cell compartments, has been extensively studied previously in a process called "lymphoid neogenesis" (as reviewed by Pitzalis et al[52]). Lymphoid neogenesis in the stomach comprises the development of B- and T-cell compartments in an extensive process that enables in situ antigen presentation and B-cell and T-cell interactions. Therefore, the biology of B cells in the stomach—as part of these structures—is very complex and uncharacterized. The resulting follicles from lymphoid neogenesis are considered tertiary lymphoid organs (also called ectopic lymphoid structures), as they contain structures that resemble those of the lymph node. The tertiary lymphoid organs contain high endothelial venule, which regulate extravasation and trafficking, follicular DCs, T follicular helper cells, and B cells and T cells that mature into effector and memory cells. The study of tertiary lymphoid organs has not been sufficiently utilized in the study of gastric carcinogenesis. Hence, future studies can begin to dissect out the cellular components of these tertiary lymphoid structures (follicles) in hopes of identifying novel therapeutic strategies against gastric metaplasia and carcinoma.

We conclude that IDO1 mediates pseudopyloric metaplasia in the stomach and associates with human gastric metaplasia and cancer. Our study provides evidence that IDO1 contributes to B-cell regulation in the inflamed gastric microenvironment, which associates with antibody production and autoimmunity. These findings prompt further investigation of autoimmunity in gastric carcinogenesis.

Supplementary Material

Note: To access the supplementary material accompanying this article, visit the online version of *Gastroenterology* at www.gastrojournal.org, and at https://doi.org/10.1053/j.gastro.2017.09.002.

References

1. Farraye FA, Odze RD, Eaden J, et al. AGA technical review on the diagnosis and management of colorectal neoplasia in inflammatory bowel disease. Gastroenterology 2010;138:746–774; 774 e1–e4; quiz e12–13.
2. Farraye FA, Odze RD, Eaden J, et al. AGA medical position statement on the diagnosis and management of colorectal neoplasia in inflammatory bowel disease. Gastroenterology 2010;138:738–745.
3. Correa P, Haenszel W, Cuello C, et al. A model for gastric cancer epidemiology. Lancet 1975;2:58–60.
4. Kim N, Park RY, Cho SI, et al. *Helicobacter pylori* infection and development of gastric cancer in Korea: long-term follow-up. J Clin Gastroenterol 2008; 42:448–454.
5. El-Zaatari M, Kao JY, Tessier A, et al. Gli1 deletion prevents Helicobacter-induced gastric metaplasia and expansion of myeloid cell subsets. PLoS One 2013; 8:e58935.
6. Munn DH, Zhou M, Attwood JT, et al. Prevention of allogeneic fetal rejection by tryptophan catabolism. Science 1998;281:1191–1193.
7. Takikawa O, Yoshida R, Kido R, et al. Tryptophan degradation in mice initiated by indoleamine 2,3-dioxygenase. J Biol Chem 1986;261:3648–3653.
8. Mezrich JD, Fechner JH, Zhang X, et al. An interaction between kynurenine and the aryl hydrocarbon receptor can generate regulatory T cells. J Immunol 2010; 185:3190–3198.
9. Nouel A, Pochard P, Simon Q, et al. B-cells induce regulatory T cells through TGF-beta/IDO production in A CTLA-4 dependent manner. J Autoimmun 2015; 59:53–60.
10. Shinde R, Shimoda M, Chaudhary K, et al. B cell-intrinsic IDO1 regulates humoral Immunity to T cell-independent antigens. J Immunol 2015;195:2374–2382.

11. Godin-Ethier J, Hanafi LA, Duvignaud JB, et al. IDO expression by human B lymphocytes in response to T lymphocyte stimuli and TLR engagement is biologically inactive. Mol Immunol 2011;49:253–259.
12. Thaker AI, Rao MS, Bishnupuri KS, et al. IDO1 metabolites activate beta-catenin signaling to promote cancer cell proliferation and colon tumorigenesis in mice. Gastroenterology 2013;145:416–425 e1−e4.
13. El-Zaatari M, Chang YM, Zhang M, et al. Tryptophan catabolism restricts IFN-gamma-expressing neutrophils and *Clostridium difficile* immunopathology. J Immunol 2014;193:807–816.
14. Baban B, Chandler P, McCool D, et al. Indoleamine 2, 3-dioxygenase expression is restricted to fetal trophoblast giant cells during murine gestation and is maternal genome specific. J Reprod Immunol 2004; 61:67–77.
15. AbuAttieh M, Rebrovich M, Wettstein PJ, et al. Fitness of cell-mediated immunity independent of repertoire diversity. J Immunol 2007;178:2950–2960.
16. Syu LJ, El-Zaatari M, Eaton KA, et al. Transgenic expression of interferon-gamma in mouse stomach leads to inflammation, metaplasia, and dysplasia. Am J Pathol 2012;181:2114–2125.
17. The Cancer Genome Atlas Research Network. Comprehensive molecular characterization of gastric adenocarcinoma. Nature 2014;513:202–209.
18. Weis VG, Sousa JF, LaFleur BJ, et al. Heterogeneity in mouse spasmolytic polypeptide-expressing metaplasia lineages identifies markers of metaplastic progression. Gut 2013;62:1270–1279.
19. Yasui H, Takai K, Yoshida R, et al. Interferon enhances tryptophan metabolism by inducing pulmonary indoleamine 2,3-dioxygenase: its possible occurrence in cancer patients. Proc Natl Acad Sci U S A 1986; 83:6622–6626.
20. Jones MA, DeWolf S, Vacharathit V, et al. Investigating B cell development, natural and primary antibody responses in Ly-6A/Sca-1 deficient mice. PLoS One 2016;11:e0157271.
21. Crouch EE, Li Z, Takizawa M, et al. Regulation of AID expression in the immune response. J Exp Med 2007; 204:1145–1156.
22. Han JH, Akira S, Calame K, et al. Class switch recombination and somatic hypermutation in early mouse B cells are mediated by B cell and Toll-like receptors. Immunity 2007;27:64–75.
23. Wrammert J, Kallberg E, Agace WW, et al. Ly6C expression differentiates plasma cells from other B cell subsets in mice. Eur J Immunol 2002;32:97–103.
24. Holmgaard RB, Zamarin D, Li Y, et al. Tumor-expressed IDO recruits and activates MDSCs in a Treg-dependent manner. Cell Rep 2015;13:412–424.
25. Stoicov C, Fan X, Liu JH, et al. T-bet knockout prevents *Helicobacter felis*-induced gastric cancer. J Immunol 2009;183:642–649.
26. Claeys D, Faller G, Appelmelk BJ, et al. The gastric H+, K+-ATPase is a major autoantigen in chronic *Helicobacter pylori* gastritis with body mucosa atrophy. Gastroenterology 1998;115:340–347.
27. Rusak E, Chobot A, Krzywicka A, et al. Anti-parietal cell antibodies—diagnostic significance. Adv Med Sci 2016; 61:175–179.
28. Bartunkova J, Kayserova J, Shoenfeld Y. Allergy and autoimmunity: parallels and dissimilarity: the yin and yang of immunopathology. Autoimmun Rev 2009; 8:302–308.
29. Gell PGH, Coombs RRA. The classification of allergic reactions underlying disease. In: Coombs RRA, Gells PGH, eds. Clinical Aspects of Immunology. Oxford, UK: Blackwell Science, 1963.
30. Kersten C, Sivertsen EA, Hystad ME, et al. BMP-6 inhibits growth of mature human B cells; induction of Smad phosphorylation and upregulation of Id1. BMC Immunol 2005;6:9.
31. Kersten C, Dosen G, Myklebust JH, et al. BMP-6 inhibits human bone marrow B lymphopoiesis—upregulation of Id1 and Id3. Exp Hematol 2006; 34:72–81.
32. Seckinger A, Meissner T, Moreaux J, et al. Bone morphogenic protein 6: a member of a novel class of prognostic factors expressed by normal and malignant plasma cells inhibiting proliferation and angiogenesis. Oncogene 2009;28:3866–3879.
33. Huse K, Bakkebo M, Oksvold MP, et al. Bone morphogenetic proteins inhibit CD40L/IL-21-induced Ig production in human B cells: differential effects of BMP-6 and BMP-7. Eur J Immunol 2011;41: 3135–3145.
34. Hagn M, Sontheimer K, Dahlke K, et al. Human B cells differentiate into granzyme B-secreting cytotoxic B lymphocytes upon incomplete T-cell help. Immunol Cell Biol 2012;90:457–467.
35. Rowley B, Tang L, Shinton S, et al. Autoreactive B-1 B cells: constraints on natural autoantibody B cell antigen receptors. J Autoimmun 2007;29:236–245.
36. Roth KA, Kapadia SB, Martin SM, et al. Cellular immune responses are essential for the development of Helicobacter felis-associated gastric pathology. J Immunol 1999;163:1490–1497.
37. Ghosh S, Hoselton SA, Schuh JM. mu-chain-deficient mice possess B-1 cells and produce IgG and IgE, but not IgA, following systemic sensitization and inhalational challenge in a fungal asthma model. J Immunol 2012; 189:1322–1329.
38. Macpherson AJ, Lamarre A, McCoy K, et al. IgA production without mu or delta chain expression in developing B cells. Nat Immunol 2001;2:625–631.
39. Perona-Wright G, Mohrs K, Taylor J, et al. Cutting edge: Helminth infection induces IgE in the absence of mu- or delta-chain expression. J Immunol 2008; 181:6697–6701.
40. Orinska Z, Osiak A, Lohler J, et al. Novel B cell population producing functional IgG in the absence of membrane IgM expression. Eur J Immunol 2002; 32:3472–3480.
41. Chen J, Trounstine M, Alt FW, et al. Immunoglobulin gene rearrangement in B cell deficient mice generated by targeted deletion of the JH locus. Int Immunol 1993; 5:647–656.

42. Zhang Y, Weck MN, Schottker B, et al. Gastric parietal cell antibodies, Helicobacter pylori infection, and chronic atrophic gastritis: evidence from a large population-based study in Germany. Cancer Epidemiol Biomarkers Prev 2013;22:821–826.
43. Ayesh MH, Jadalah K, Al Awadi E, et al. Association between vitamin B12 level and anti-parietal cells and anti-intrinsic factor antibodies among adult Jordanian patients with Helicobacter pylori infection. Braz J Infect Dis 2013;17:629–632.
44. Bergman MP, Faller G, D'Elios MM, et al. Gastric autoimmunity. In: Mobley HLT, Mendz GL, Hazell SL, eds. *Helicobacter pylori: Physiology and Genetics*. Washington, DC: American Society for Microbiology, 2001.
45. Sterzl I, Hrda P, Matucha P, et al. Anti-Helicobacter Pylori, anti-thyroid peroxidase, anti-thyroglobulin and anti-gastric parietal cells antibodies in Czech population. Physiol Res 2008;57(Suppl 1):S135–S141.
46. Sugiu K, Kamada T, Ito M, et al. Anti-parietal cell antibody and serum pepsinogen assessment in screening for gastric carcinoma. Dig Liver Dis 2006; 38:303–307.
47. Lo CC, Hsu PI, Lo GH, et al. Implications of anti-parietal cell antibodies and anti-*Helicobacter pylori* antibodies in histological gastritis and patient outcome. World J Gastroenterol 2005;11:4715–4720.
48. Bonilla Palacios JJ, Miyazaki Y, Kanayuma S, et al. Serum gastrin, pepsinogens, parietal cell and *Helicobacter pylori* antibodies in patients with gastric polyps. Acta Gastroenterol Latinoam 1994; 24:77–82.
49. Strong MJ, Xu G, Coco J, et al. Differences in gastric carcinoma microenvironment stratify according to EBV infection intensity: implications for possible immune adjuvant therapy. PLoS Pathog 2013; 9:e1003341.
50. Kim SY, Park C, Kim HJ, et al. Deregulation of immune response genes in patients with Epstein-Barr virus-associated gastric cancer and outcomes. Gastroenterology 2015;148:137–147 e9.
51. Scott GN, DuHadaway J, Pigott E, et al. The immunoregulatory enzyme IDO paradoxically drives B cell-mediated autoimmunity. J Immunol 2009; 182:7509–7517.
52. Pitzalis C, Jones GW, Bombardieri M, et al. Ectopic lymphoid-like structures in infection, cancer and autoimmunity. Nat Rev Immunol 2014;14:447–462.

Received June 8, 2016. Accepted September 2, 2017.

Reprint requests
Address requests for reprints to: Mohamad El-Zaatari, PhD, Department of Internal Medicine-Gastroenterology, University of Michigan, 6518 MSRB 1, 1150 W Medical Center Drive, Ann Arbor, Michigan 48109-5682. e-mail: mohamade@med.umich.edu; fax: (734) 763-2535 or John Y. Kao, MD, Department of Internal Medicine-Gastroenterology, University of Michigan, 6520A MSRB 1, 1150 W Medical Center Drive, Ann Arbor, Michigan 48109-5682. e-mail: jykao@med.umich.edu; fax: (734) 763-2535.

Acknowledgments
The authors would like to acknowledge the American Gastroenterological Association/Gastric Cancer Foundation for providing grant N017489 (El-Zaatari), which supported this study. Additionally, the authors would like to acknowledge Department of Defense grant CA160431 (El-Zaatari) for supporting the final stages of this study. The authors would also like to acknowledge the National Institutes of Health for Public Health Service grants National Institute of Diabetes and Digestive and Kidney Diseases R01 DK087708-01 (Kao); 5P30DK034933 (Owyang); University of Michigan Comprehensive Cancer John S. and Suzanne C. Munn Cancer Fund (Todisco); DK062041 and CA118875 (Dlugosz), which also supported this study.

Conflicts of interest
The authors disclose no conflicts.

Funding
This study was supported by the American Gastroenterological Association/Gastric Cancer Foundation grant N017489 (El-Zaatari); Department of Defense grant CA160431 (El-Zaatari); Public Health Service grants National Institute of Diabetes and Digestive and Kidney Diseases grants R01 DK087708-01 (Kao); 5P30DK034933 (Owyang); University of Michigan Comprehensive Cancer John S. and Suzanne C. Munn Cancer Fund (Todisco), DK062041 and CA118875 (Dlugosz).

Supplementary Methods

Helicobacter felis *Infection*

The CS1 strain of *H felis* was cultured in Brucella broth (BD, Franklin Lakes, NJ) plus 10% fetal bovine serum (Atlanta Biologicals, Lawrenceville, GA) with 150 rpm shaking using the GasPak EZ Campy Container System (BD) at 37°C. Mice were gavaged with 10^8 *H felis* cells in 100 μL Brucella broth 3 times, once every other day. Control mice were gavaged with Brucella broth lacking *H felis*.

Tissue Collection

The stomachs were opened along the greater curvature and washed in phosphate-buffered saline. The stomach weight was measured and normalized to total body weight. The tissue was processed as follows for each application:

1. For histology, gastric strips from both the lesser and greater curvatures were fixed in formalin for paraffin sections, or frozen at −80°C in OCT for frozen sections.
2. For flow cytometry, gastric cells were digested using a modified version of the protocol described by Geem et al.[1] This protocol was described previously[2] and utilizes 17.9 μg/mL Liberase TM (Cat #05401119001; Roche Diagnostics Corporation, Indianapolis, IN) instead of type VIII collagenase.
3. For RNA extraction, samples spanning the fundus/corpus were homogenized in TRIzol (Invitrogen, Carlsbad, CA) and cleaned up using the RNEasy Microkit (Qiagen), as we described previously.[3]
4. For DNA, gastric tissue was snap frozen in liquid nitrogen and extracted using the DNEasy Blood and Tissue Kit (Qiagen).
5. For mass spectrometry, the tissue was homogenized in a solution consisting of 4 mM sodium metabisulfite, 1 mM EDTA, and 0.01 N HCl, to acidify and prevent the tryptophan from oxidizing. The homogenized sample was stored at −80°C. For each analysis, the tissue segments were collected from equivalent positions within the stomachs of different mice.

Pathologic Scoring of Metaplasia, Parietal Cell Loss

The criteria for detecting spasmolytic peptide-expressing metaplasia were described previously,[4,5] spasmolytic peptide-expressing metaplasia was quantified by immunofluorescent colocalization of trefoil factor 2 (TFF-2) and intrinsic factor as shown in Supplementary Figure 3*A*. Four strips of gastric mucosa for each mouse (2 from lesser and 2 from greater curvatures) were sectioned in paraffin blocks and stained with TFF-2 and intrinsic factor. The 20× images were captured spanning the entire sections by confocal microscopy. The percentage area of metaplasia was calculated by dividing the number of 20× focal planes containing metaplasia over the total number of captured 20× focal planes spanning the entire fundic/corpus section for each mouse. For parietal cell quantification, the number of parietal cells (Supplementary Figure 3*B*) was quantified using Fiji (ImageJ).[6] This was performed by converting single channel parietal cell staining into binary black and white color. The number of parietal cells was normalized over the total glandular area. The analysis was performed over the entire sections spanning 4 histologic strips (2 from lesser and 2 from greater curvatures) for each mouse.

Immunofluorescence and Antibodies

Immunofluorescence on frozen and paraffin sections was performed as described previously.[7] The following antibodies were used for immunofluorescence: polyclonal goat anti-mouse IDO1 (I-17 cat. #sc-25121; Santa Cruz Biotechnology, Santa Cruz, CA); intrinsic factor (gift from David Alpers, Washington University, St Louis, MO); H^+/K^+-ATPase-β (#D032-3; Medical and Biological Laboratories, Woburn, MA); B220-AlexaFluor 647 (clone RA3-6B2, cat. #103229; BioLegend); E-cadherin−fluorescein isothiocyanate (#612130, BD Biosciences, San Jose, CA). For immunohistochemical double staining of NK cells and parietal cells, purified NK1.1 antibody (clone PK136, cat. #108712; BioLegend) was horseradish peroxidase−conjugated using the Abcam horseradish peroxidase conjugation kit (catalog #ab102890; Abcam, Cambridge, MA) and developed using 4′,6-diamidino-2-phenylindole. H^+/K^+-ATPase-β antibody (#D032-3; MBL, Woburn, MA) was then applied overnight, followed by horseradish peroxidase−conjugated secondary antibody, and the staining briefly developed using a 5-second incubation period with Vector VIP (catalog #SK-4600, Vector Laboratories, Burlingame, CA).

Quantitative Polymerase Chain Reaction and Real-Time Quantitative Polymerase Chain Reaction

For DNA quantification of *H felis* flagellar filament B (Fla-B), quantitative PCR was performed on a CFX96 real-time PCR detection system using the following primers:

Fla-B Forward 5′- TTCGATTGGTCCTACAGGCTCAGA-3′
Fla-B Reverse 5′- TTCTTGTTGATGACATTGACCAACGCA-3′

The method used for qPCR quantification and the RT-qPCR primers for interleukin-1β, IFN-gamma, tumor necrosis factor−α, and interleukin-12p40 was described previously.[7] The other RT-qPCR primers were as follows:

IDO1 Forward 5′- TGGCGTATGTGTGGAACCGA -3′
IDO1 Reverse 5′- GGCAGGCCCAACTTCTCTGA -3′
CD79a Forward 5′- GGGATCATCTTGCTGTTCTGTGC -3′
CD79a Reverse 5′- AGTCATCTGGCATGTCCACCC -3′
Igk v1-133 Forward 5′- TGATGAGTCCTGCCCAGTTCC -3′
Igk v1-133 Reverse 5′- TGGTTGTCCAATGGTAACCGAC -3′
Blimp-1 Forward 5′- ACACAGTTCCCAAGAATGCCAAC -3′
Blimp-1 Reverse 5′- TTGCTTTTCTCCTCATTAAAGCCATC -3′

The human RT-qPCR primer sequences for GAPDH (PPH00150F), TFF-2 (PPH07174A), CD44 (PPH00114A),

IFNG (PPH00380C), and IL1B (PPM03109E) were performed using the Qiagen RT2 qPCR Primer Assay (cat. #330001). Furthermore, the IDO1 human RT-qPCR primer sequence was designed as follows:

Human IDO1 Forward 5′- GGCACCAGAGGAGCAGACTA CAA -3′

Human IDO1 Reverse 5′- ACTCTTTCTCGAAGCTGGCCA GAC -3′

Mass Spectrometry

Mass spectrometry was performed by the Michigan Regional Comprehensive Metabolomics Resource Core. Gastric tissue was homogenized in 4 mM sodium metabisulfite, 1 mM EDTA, and 0.01 N HCl, to acidify and prevent the tryptophan from oxidizing. The homogenized sample was stored at −80°C until use. Mass spectrometry was performed as described previously.[2]

Microarray Analysis and Comparison to The Cancer Genome Atlas Datasets

The mouse gene lists were converted to human homologs using online software developed by the University of Washington called MammalHom. Gene comparisons with the human clusters were performed using online software developed by the Whitehead Institute (Massachusetts Institute of Technology) (http://jura.wi.mit.edu/bioc/tools/compare.php). The human gene lists were obtained from TCGA.[8] Heatmaps were constructed using MeV (Microarray Software Suite, Dana-Farber Cancer Institute, Boston, MA).

Mouse Anti-Gastric Parietal Cell Enzyme-Linked Immunosorbent Assay

Mouse plasma was collected in K3 EDTA. Mouse anti-gastric parietal cell enzyme-linked immunosorbent assay was performed using a commercial kit (cat. #MBS7240770; MyBioSource, San Diego, CA) according to the manufacturer's instructions.

References

1. Geem D, Medina-Contreras O, Kim W, et al. Isolation and characterization of dendritic cells and macrophages from the mouse intestine. J Vis Exp 2012:e4040.
2. El-Zaatari M, Chang YM, Zhang M, et al. Tryptophan catabolism restricts IFN-gamma-expressing neutrophils and *Clostridium difficile* immunopathology. J Immunol 2014;193:807–816.
3. Essien BE, Grasberger H, Romain RD, et al. ZBP-89 regulates expression of tryptophan hydroxylase I and mucosal defense against *Salmonella typhimurium* in mice. Gastroenterology 2013;144:1466–1477, 1477 e1−e9.
4. Nozaki K, Ogawa M, Williams JA, et al. A molecular signature of gastric metaplasia arising in response to acute parietal cell loss. Gastroenterology 2008;134:511–522.
5. Goldenring JR, Nam KT, Mills JC. The origin of pre-neoplastic metaplasia in the stomach: chief cells emerge from the Mist. Exp Cell Res 2011;317:2759–2764.
6. Schindelin J, Arganda-Carreras I, Frise E, et al. Fiji: an open-source platform for biological-image analysis. Nat Methods 2012;9:676–682.
7. El-Zaatari M, Kao JY, Tessier A, et al. Gli1 deletion prevents Helicobacter-induced gastric metaplasia and expansion of myeloid cell subsets. PLoS One 2013;8:e58935.
8. Cancer Genome Atlas Research Network. Comprehensive molecular characterization of gastric adenocarcinoma. Nature 2014;513:202–209.

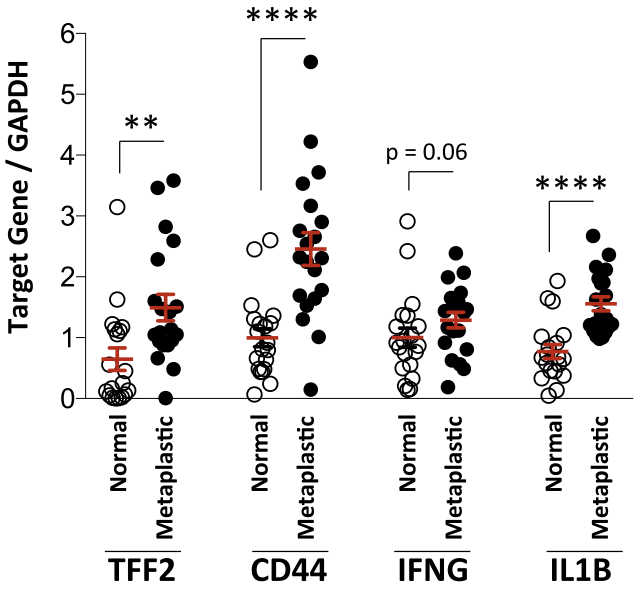

Supplementary Figure 1. Induction of spasmolytic peptide-expressing metaplasia (SPEM) markers in the lesser curvature of human metaplastic stomachs. RT-qPCR of *TFF-2*, *CD44*, *IFNG*, and *IL1B* in metaplastic stomachs (lesser curvature) vs normal. Each data point represents 1 patient sample. n = 20 patients per group. $^{**}P < .01$; $^{****}P < .0001$.

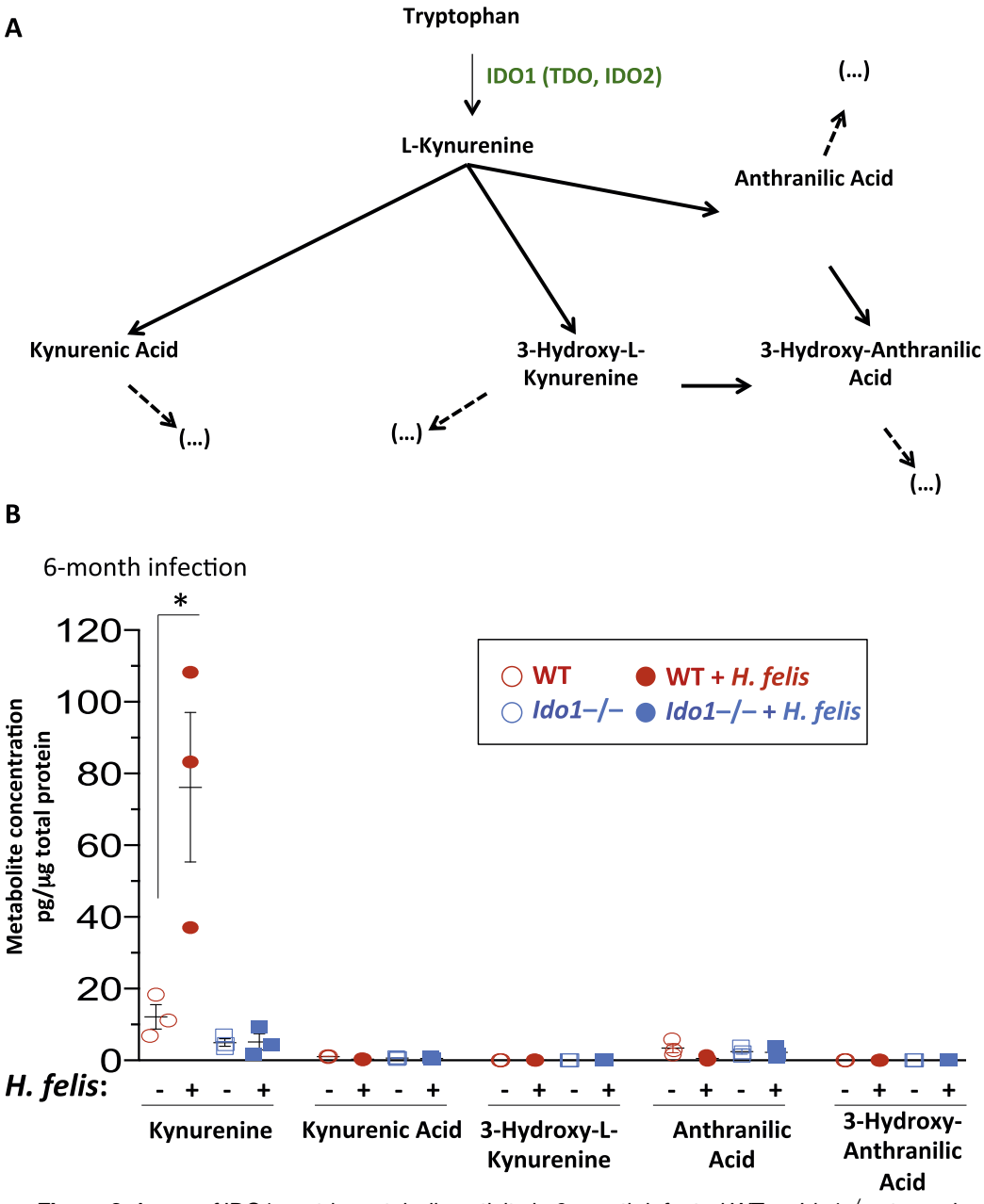

Supplementary Figure 2. Assay of IDO1 gastric metabolic activity in 6-month infected WT vs *Ido1*$^{-/-}$ stomachs. (*A*) Metabolic pathway of tryptophan catabolism by IDO1. (*B*) Mass spectrometric (liquid chromatography–mass spectrometry) measurements of gastric tissue levels of IDO1 metabolites in 6-month *H felis*–infected WT vs *Ido1*$^{-/-}$ mice (and uninfected controls). Values are normalized to micrograms of total gastric protein in the analyzed sample. Each data point represents 1 mouse. Error bars represent the means ± SEM. *$P < .05$.

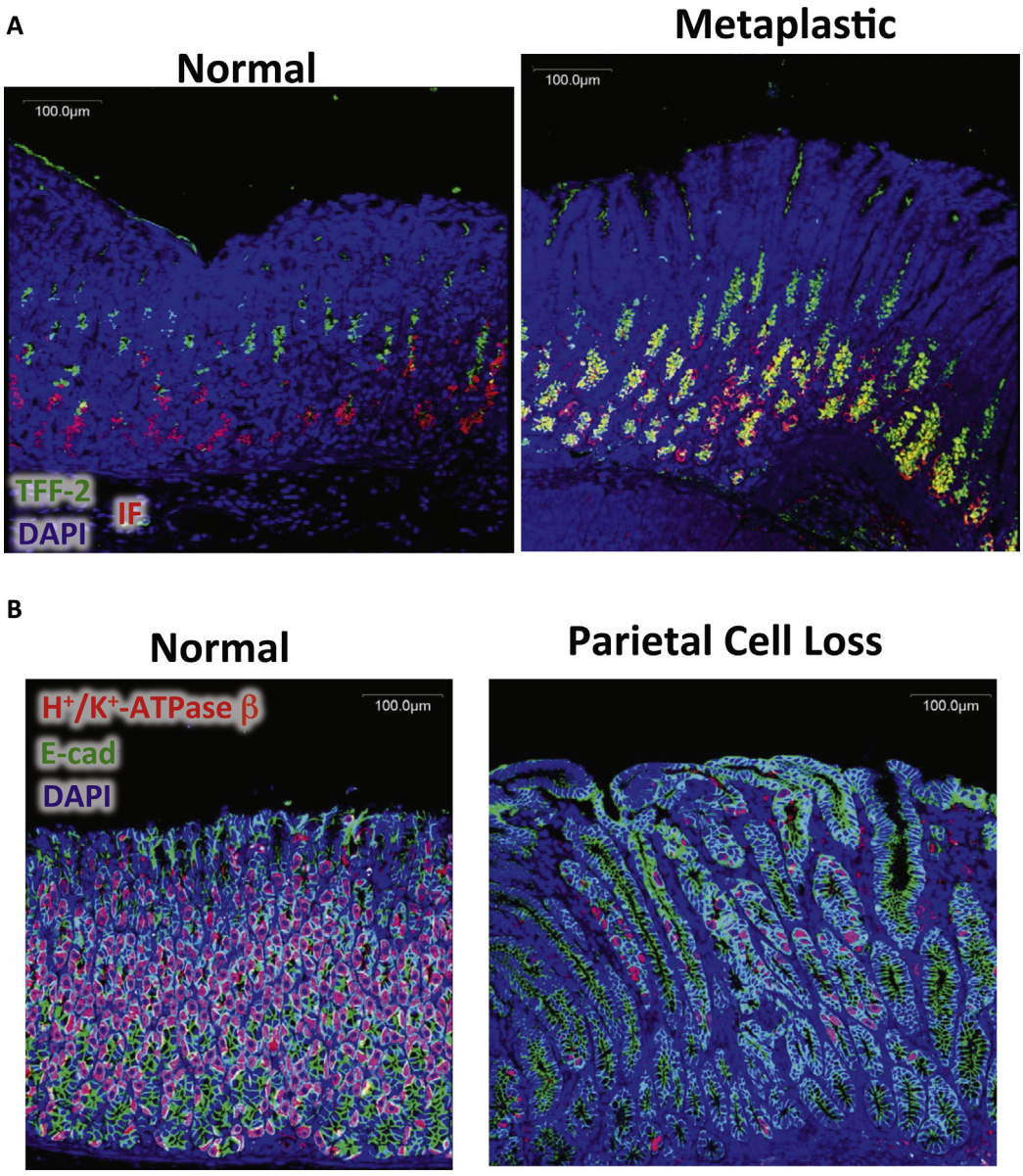

Supplementary Figure 3. Criteria for quantifying pseudopyloric metaplasia (SPEM) and parietal cell loss. (*A*) Confocal microscopy showing trefoil factor 2 (TFF-2, *green*), intrinsic factor (IF, *red*), and 4′,6-diamidino-2-phenylindole (DAPI) (*blue*). The colocalization of TFF-2 and IF indicate a metaplastic epithelium, whereas lack of colocalization indicate a normal epithelium. The *image* illustrates the difference in normal vs metaplastic gastric mucosal tissue that was used for scoring (the scoring is described in the Methods section). (*B*) Confocal microscopy showing H^+/K^+-ATPase β (*red*), E-cadherin (*green*), and DAPI (*blue*). The *image* illustrates the difference between normal mucosa vs parietal cell loss that was used for scoring (the scoring is described in the Methods section).

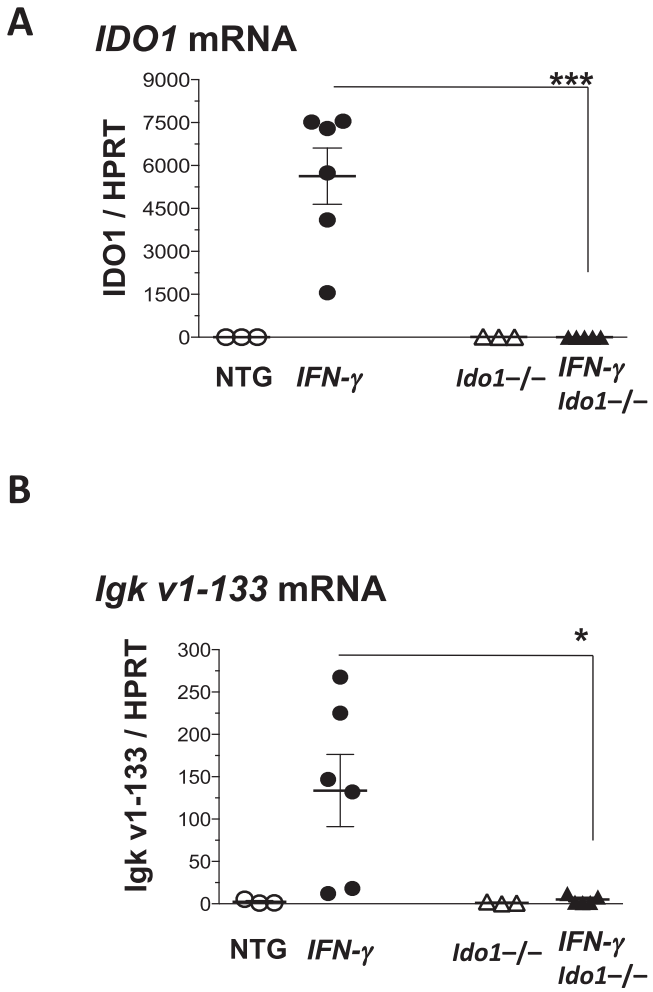

Supplementary Figure 4. IDO1 deficiency reduces B-cell marker expression in the IFN-gamma–overexpressing model. (*A*) RT-qPCR of *IDO1* mRNA in *IFN-gamma* vs *IFN-gamma-Ido1*$^{-/-}$ stomachs, relative to non-transgenic controls. (*B*) RT-qPCR of *Igk v1-133* in *IFN-gamma* vs *IFN-gamma-Ido1*$^{-/-}$ stomachs, relative to non-transgenic controls. Each data point represents 1 mouse. Error bars represent the mean ± SEM. **P* < .05; ****P* < .001.

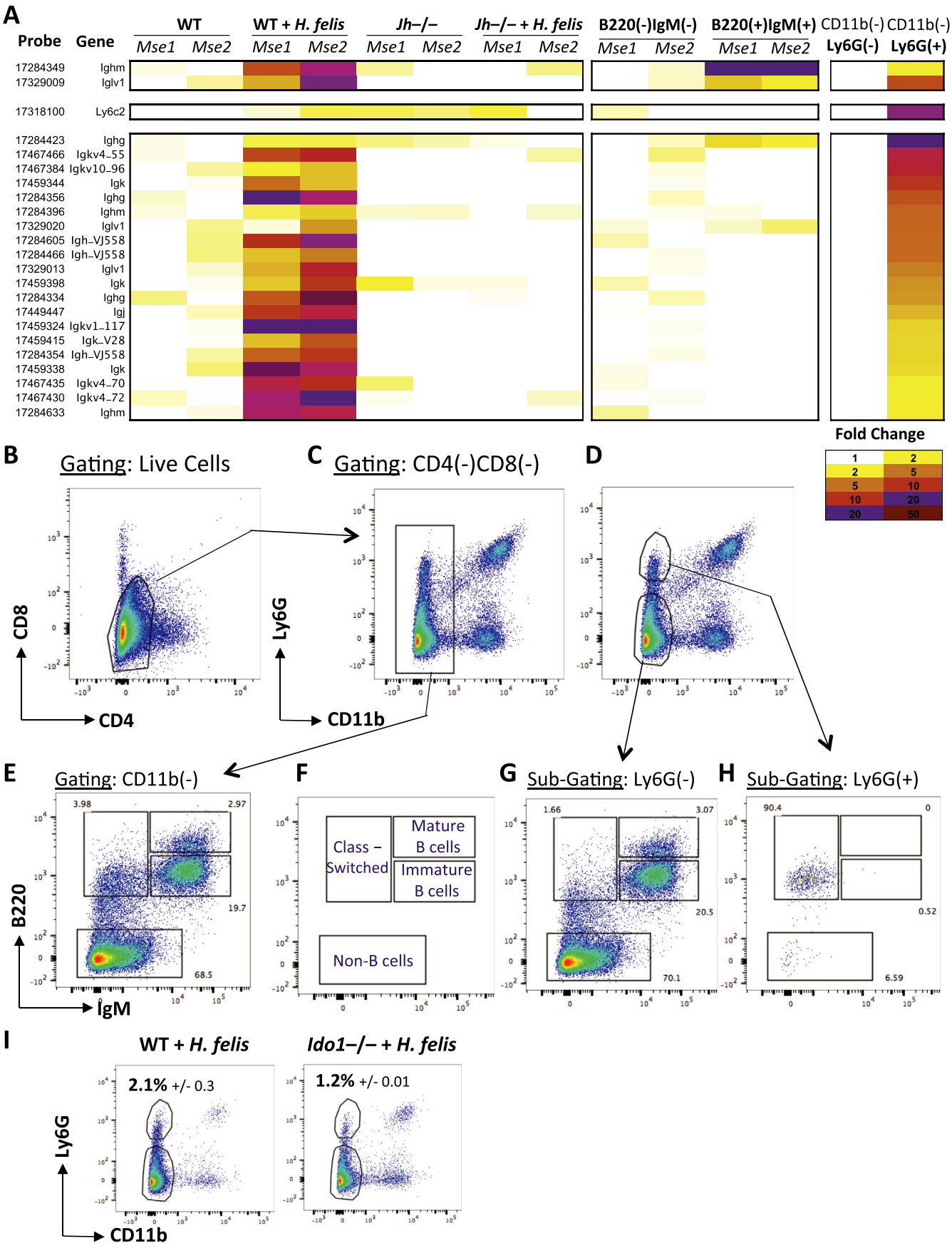
A
Probe
Gene
WT
WT + H. felis
Jh–/–
Jh–/– + H. felis
B220(-)IgM(-)
B220(+)IgM(+)
CD11b(-) Ly6G(-)
CD11b(-) Ly6G(+)
Mse1
Mse2
17284349 Ighm
17329009 Iglv1
17318100 Ly6c2
17284423 Ighg
17467466 Igkv4_55
17467384 Igkv10_96
17459344 Igk
17284356 Ighg
17284396 Ighm
17329020 Iglv1
17284605 Igh_VJ558
17284466 Igh_VJ558
17329013 Iglv1
17459398 Igk
17284334 Ighg
17449447 Igj
17459324 Igkv1_117
17459415 Igk_V28
17284354 Igh_VJ558
17459338 Igk
17467435 Igkv4_70
17467430 Igkv4_72
17284633 Ighm
Fold Change
1
2
5
10
20
50
B
Gating: Live Cells
CD8
CD4
C
Gating: CD4(-)CD8(-)
Ly6G
CD11b
D
E
Gating: CD11b(-)
B220
IgM
3.98
2.97
19.7
68.5
F
Class – Switched
Mature B cells
Immature B cells
Non-B cells
G
Sub-Gating: Ly6G(-)
1.66
3.07
20.5
70.1
H
Sub-Gating: Ly6G(+)
90.4
0
0.52
6.59
I
WT + H. felis
Ido1–/– + H. felis
2.1% +/- 0.3
1.2% +/- 0.01
Ly6G
CD11b

Supplementary Figure 5. Identification of class-switched B cells, which are not increased in 6-month infected *Ido1*$^{-/-}$ mice relative to WT. (A) *Left panel:* Microarray heatmap of immunoglobulin cassette genes from total stomach RNA of WT vs B-cell–deficient (*Jh*$^{-/-}$) stomachs ± *H felis*. *Middle panel:* Microarray heatmap of immunoglobulin cassette genes in FACS-isolated naïve B cells (B220^{+}IgM^{+}) vs non-B cells (B220^{-}IgM^{-}). *Right panel:* Microarray heatmap of immunoglobulin gene cassette genes and *Ly6c2* in FACS-isolated CD11b^{-}Ly6G^{+} immune cells vs CD11b^{-}Ly6G^{-} cells. (*B*) Negative sub-gating of total live gastric cells to exclude CD8^{+} and CD4^{+} T cells. (*C, D*) Negative sub-gating of CD4^{-}CD8^{-} live cells to further exclude CD11b^{+} myeloid cells. (*E*) FACS analysis of CD4^{-}CD8^{-}CD11b^{-} live gastric mucosa cells for IgM (x-axis) and B220 (y-axis) marker expression. The populations are divided into IgM^{+}B220^{low} (immature naïve B cells), IgM^{+}B220^{high} (mature naïve B cells), IgM^{-}B220^{+} (class-switched B cells), and IgM^{-}B220^{-} (non-B cells). (*F*) Labeling of different sub-gates in (*E*). (*G*) Sub-gating of Ly6G^{-} (CD4^{-}CD8^{-}CD11b^{-}) immune cells according to IgM (x-axis) and B220 (y-axis) marker expression. (*H*) Sub-gating of Ly6G^{+} (CD4^{-}CD8^{-}CD11b^{-}) immune cells according to IgM (x-axis) and B220 (y-axis) marker expression. (*I*) FACS analysis of class-switched Ly6G^{+} (CD4^{-}CD8^{-}CD11b^{-}) B cells in 6-month infected WT vs *Ido1*$^{-/-}$ stomachs. The percentage is expressed as a proportion of total live CD4^{-}CD8^{-} gastric cells.

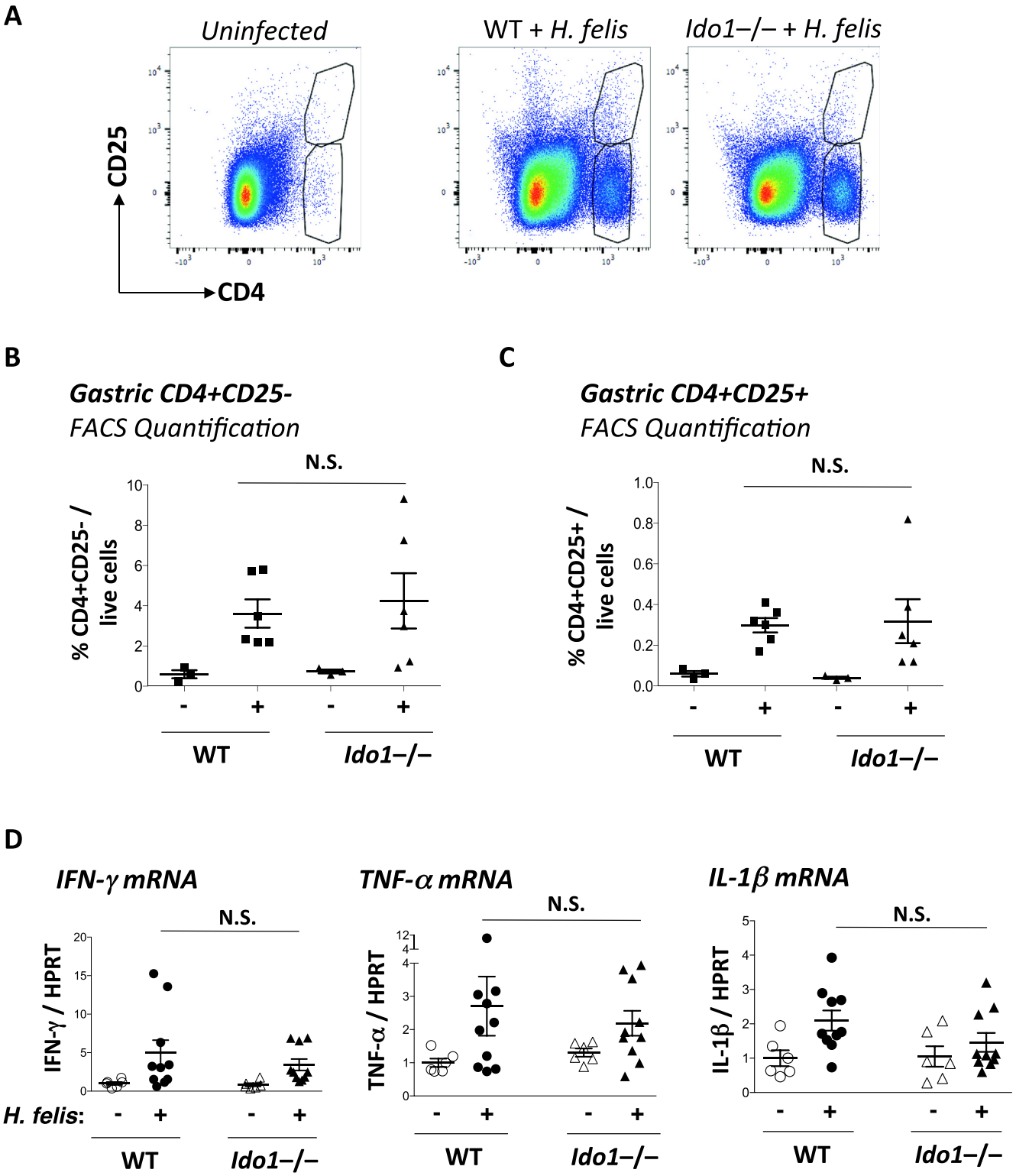

Supplementary Figure 6. Quantification of gastric T cells and T-helper 1–associated cytokines in 6-month *H felis*–infected WT vs *Ido1*$^{-/-}$. (*A*) Representative FACS plots of gastric CD4^{+}CD25^{+} and CD4^{+}CD25^{-} cells isolated from 6-month *H felis*–infected WT vs *Ido1*$^{-/-}$ stomachs, as compared to an uninfected stomach control. (*B*) Graphical representation of CD4^{+}CD25^{-} percentages from uninfected and 6-month *H felis*–infected WT vs *Ido1*$^{-/-}$ stomachs. (*C*) Graphical representation of CD4^{+}CD25^{+} percentages from uninfected and 6-month *H felis*–infected WT vs *Ido1*$^{-/-}$ stomachs. (*D*) RT-qPCR analysis of *IFN-gamma*, *TNF-α*, and *IL-1β* mRNA between WT and *Ido1*$^{-/-}$ stomachs ± 6-month *H felis* infection. Each data point represents 1 mouse. *Error bars* represent the mean and SEM. NS, not significant.

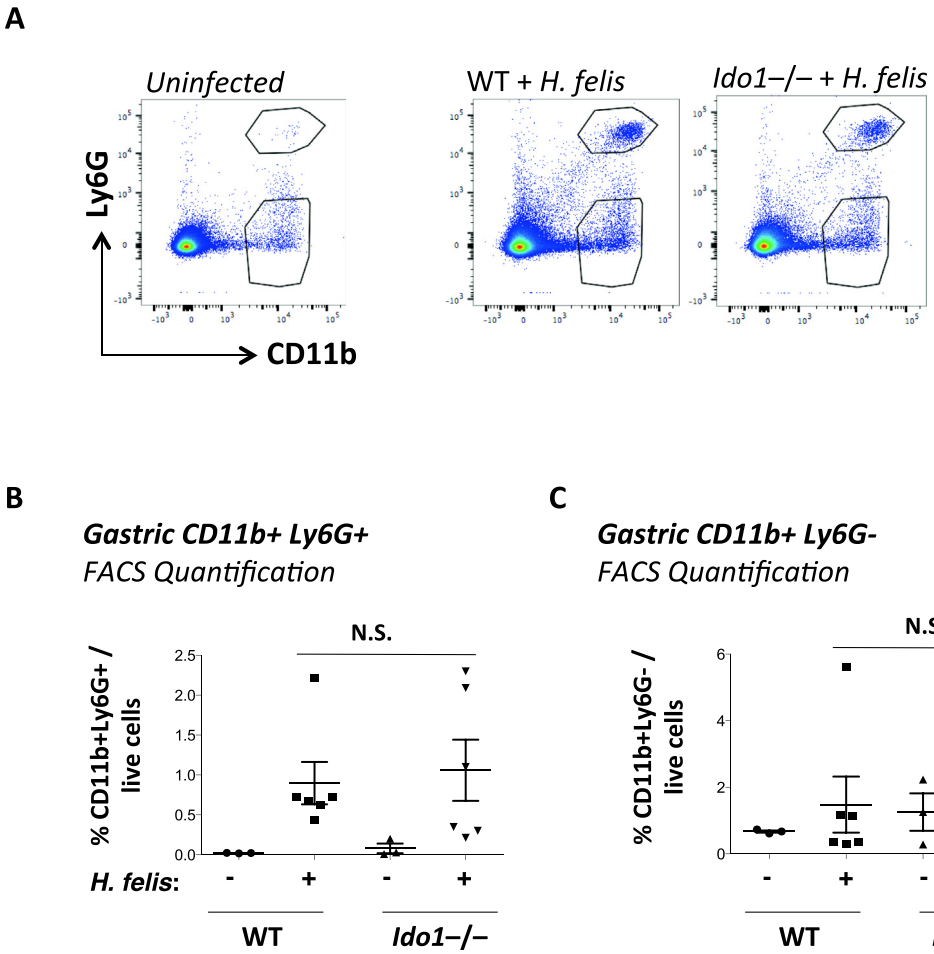

Supplementary Figure 7. Quantification of gastric myeloid cells. (*A*) Representative FACS plots of CD11b^{+}Ly6G^{-} myeloid cells and CD11b^{+}Ly6G^{+} MDSCs from uninfected and 6-month *H felis*–infected WT vs *Ido1*$^{-/-}$ stomachs. (*B*) Graphical representation of FACS percentages of CD11b^{+}Ly6G^{+} MDSCs from 6-month *H felis*–infected WT vs *Ido1*$^{-/-}$ stomachs. (*C*) Graphical representation of FACS percentages of CD11b^{+}Ly6G^{-} cells from 6-month *H felis*–infected WT vs *Ido1*$^{-/-}$ stomachs. Each data point represents 1 mouse. Error bars represent the mean ± SEM. NS, not significant.

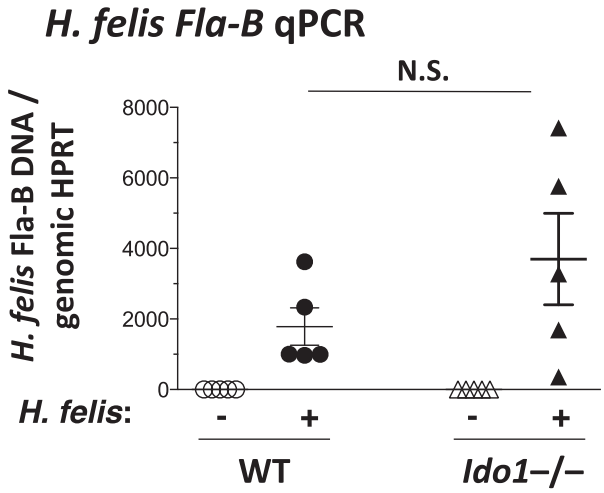

Supplementary Figure 8. Lack of significant change in *H felis* DNA between *H felis*–infected WT vs *Ido1*$^{-/-}$ stomachs. qPCR quantification of flagellar filament B (*Fla-B* DNA) in WT vs *Ido1*$^{-/-}$ stomachs ± 6-month *H felis* infection. Each data point represents 1 mouse. Error bars represent the mean ± SEM. NS, not significant.

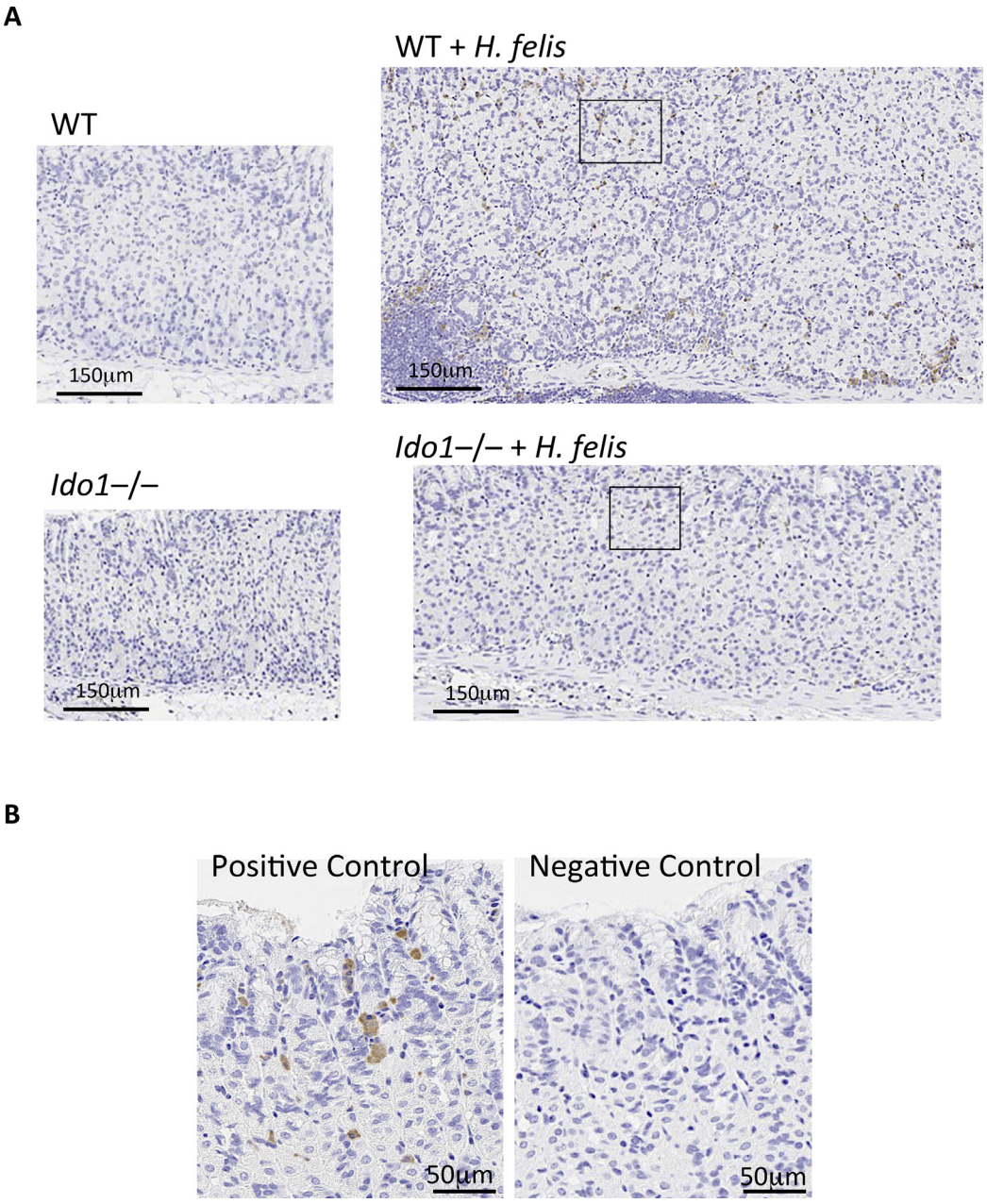

Supplementary Figure 9. NK1.1-HRP staining in WT vs *Ido1*$^{-/-}$ gastric tissue ± *H felis*. (*A*) Immunohistochemical staining of NK1.1-HRP in WT vs *Ido1*$^{-/-}$ gastric tissue ± *H felis*. The *black boxes* represent the insets used for Figure 3*B*. (*B*) Negative vs positive control staining of NK1.1-HRP in consecutive sections from a 6-month *H felis*–infected WT stomach.

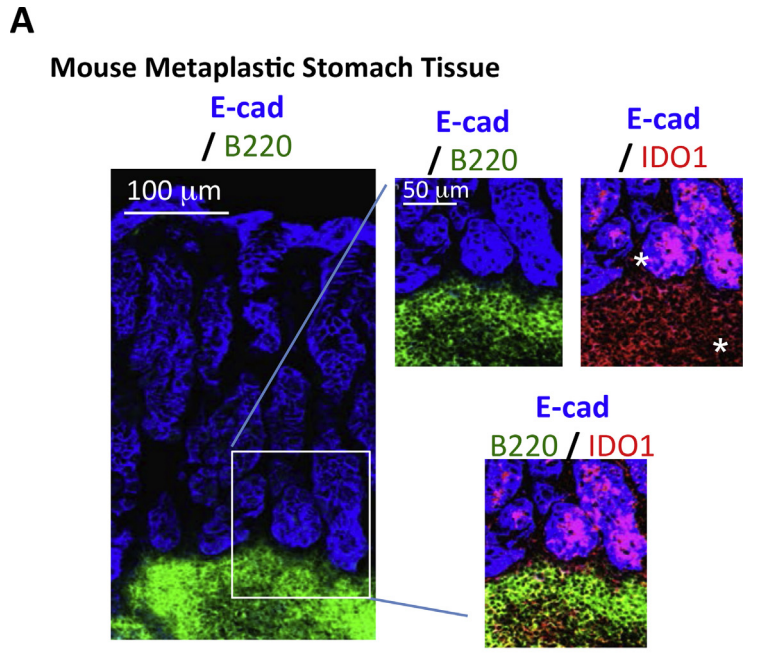

Supplementary Figure 10. IDO1 is expressed by epithelial cells and B cells in metaplastic mouse stomach and chronically inflamed human stomach. (*A*) Immunofluorescent staining of IDO1 (*red*), B220 (*green*), and E-cadherin (*blue*) from a 6-month *H felis* −infected WT stomach. (*B*) Immunohistochemistry of IDO1 (*brown*) from human metaplastic stomach tissue using the Biomax gastric tissue microarray panel. The tissue section was counterstained with hematoxylin. (*C*) Immunohistochemistry of IDO1 (*brown*) in a human gastric cancer tissue section (from the Biomax gastric tissue microarray panel).

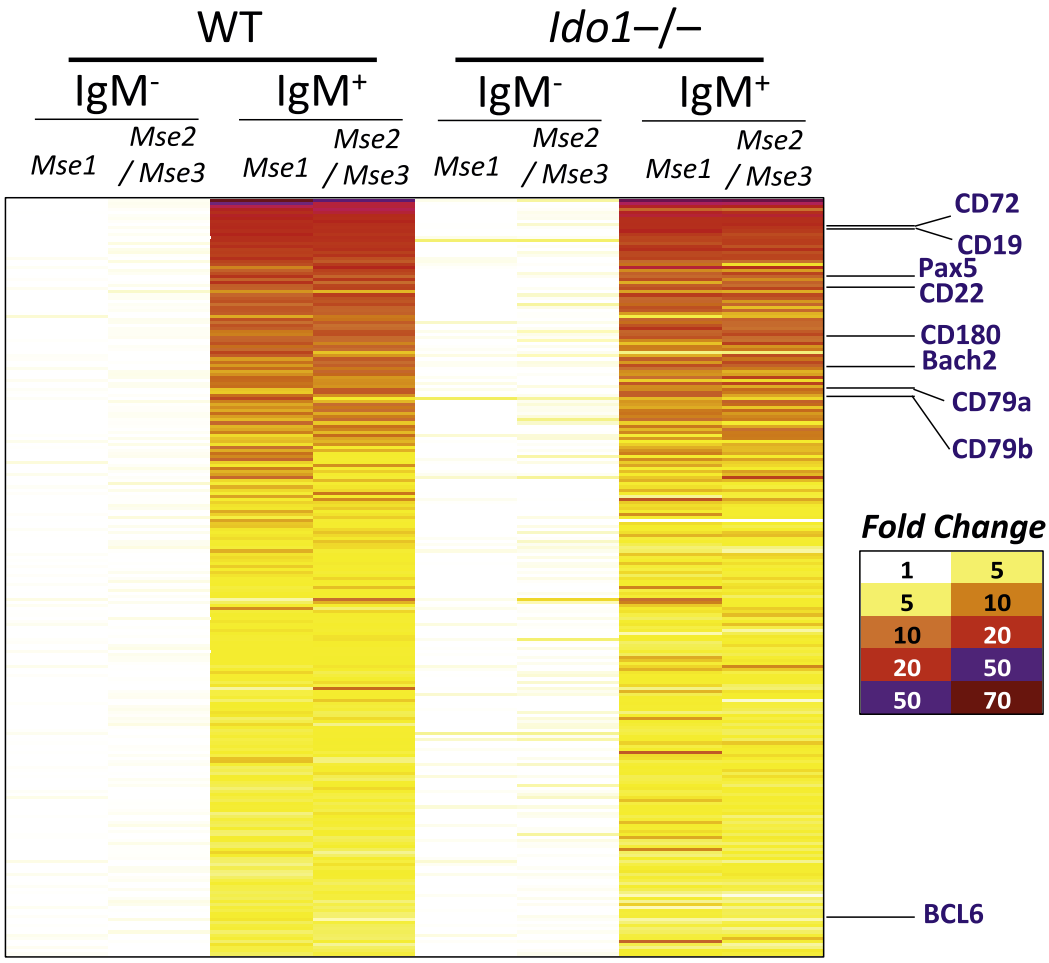

Supplementary Figure 11. Microarray heatmap of isolated gastric B cells vs non-B cells from 6-month infected WT and *Ido1*$^{-/-}$ stomachs. The annotations represent B-cell marker genes enriched in the isolated populations. "Mse 1" refers to isolated RNA from gastric B cells of one mouse, whereas "Mse 2/Mse 3" represents pooled isolated RNA from gastric B cells of 2 mice to serve as a replicate.

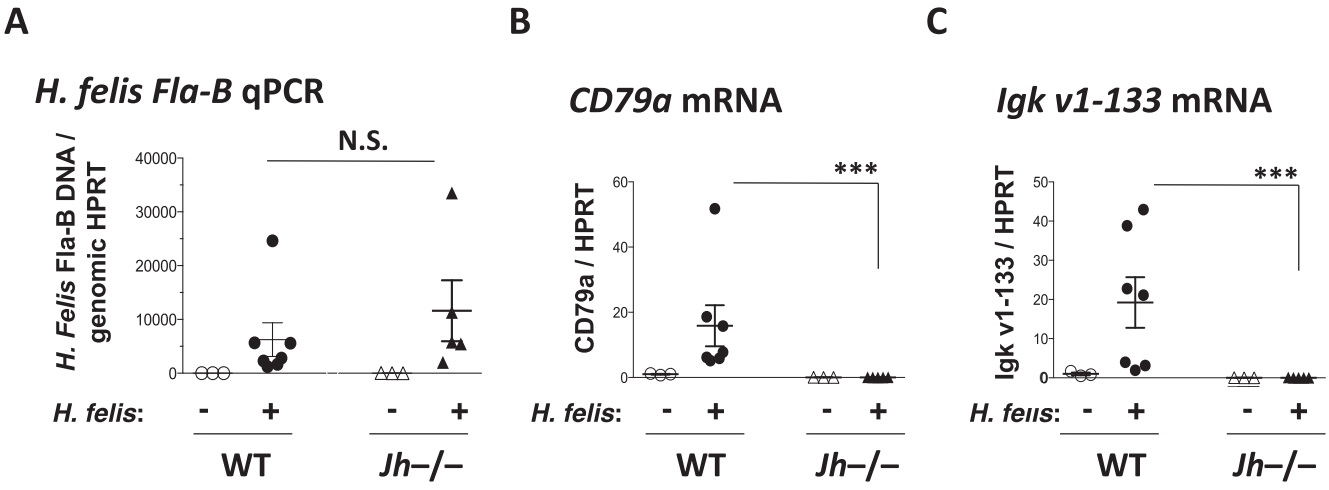

Supplementary Figure 12. Validation of B-cell deficiency in *Jh*$^{-/-}$ mice, and lack of significant changes in *H felis* DNA. (*A*) qPCR quantification of *H felis* flagellar filament B (*Fla-B*) DNA. (*B, C*) RT-qPCR analysis of B cell markers (*CD79a* and *Igk v1-133*). Each data point represents 1 mouse. Error bars represent the mean ± SEM. ***$P < .001$. NS, not significant.

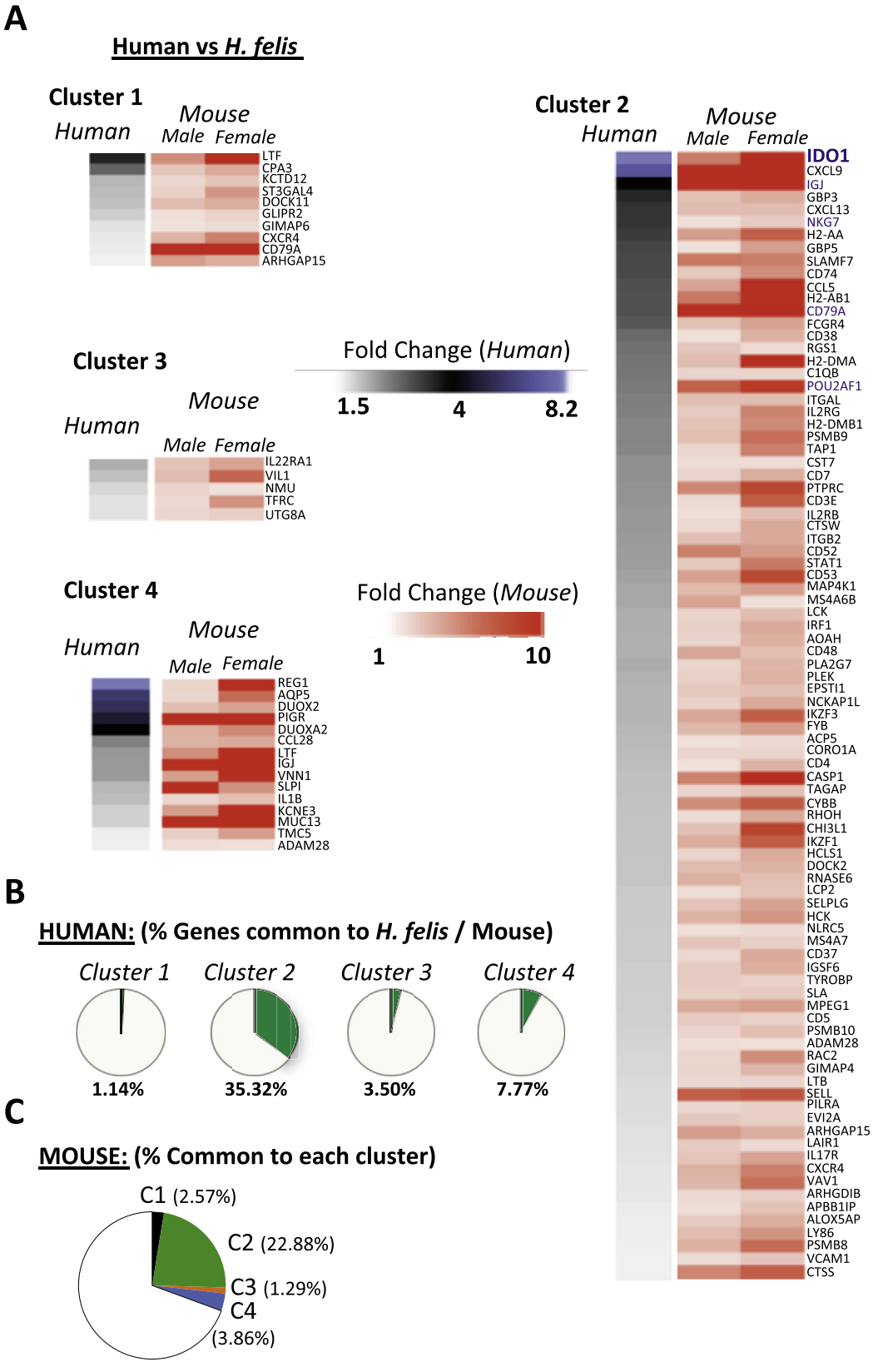
A
Human vs H. felis
Cluster 1
Human
Mouse
Male Female
LTF
CPA3
KCTD12
ST3GAL4
DOCK11
GLIPR2
GIMAP6
CXCR4
CD79A
ARHGAP15
Cluster 2
Human
Mouse
Male Female
IDO1
CXCL9
IGJ
GBP3
CXCL13
NKG7
H2-AA
GBP5
SLAMF7
CD74
CCL5
H2-AB1
CD79A
FCGR4
CD38
RGS1
H2-DMA
C1QB
POU2AF1
ITGAL
IL2RG
H2-DMB1
PSMB9
TAP1
CST7
CD7
PTPRC
CD3E
IL2RB
CTSW
ITGB2
CD52
STAT1
CD53
MAP4K1
MS4A6B
LCK
IRF1
AOAH
CD48
PLA2G7
PLEK
EPSTI1
NCKAP1L
IKZF3
FYB
ACP5
CORO1A
CD4
CASP1
TAGAP
CYBB
RHOH
CHI3L1
IKZF1
HCLS1
DOCK2
RNASE6
LCP2
SELPLG
HCK
NLRC5
MS4A7
CD37
IGSF6
TYROBP
SLA
MPEG1
CD5
PSMB10
ADAM28
RAC2
GIMAP4
LTB
SELL
PILRA
EVI2A
ARHGAP15
LAIR1
IL17R
CXCR4
VAV1
ARHGDIB
APBB1IP
ALOX5AP
LY86
PSMB8
VCAM1
CTSS
Cluster 3
Human
Mouse
Male Female
IL22RA1
VIL1
NMU
TFRC
UTG8A
Fold Change (Human)
1.5
4
8.2
Cluster 4
Human
Mouse
Male Female
REG1
AQP5
DUOX2
PIGR
DUOXA2
CCL28
LTF
IGJ
VNN1
SLPI
IL1B
KCNE3
MUC13
TMC5
ADAM28
Fold Change (Mouse)
1
10
B
HUMAN: (% Genes common to H. felis / Mouse)
Cluster 1
Cluster 2
Cluster 3
Cluster 4
1.14%
35.32%
3.50%
7.77%
C
MOUSE: (% Common to each cluster)
C1 (2.57%)
C2 (22.88%)
C3 (1.29%)
C4
(3.86%)

Supplementary Figure 13. Common genes induced in the *H felis* model and the human gastric adenocarcinoma expression clusters. (*A*) Fold-change heatmaps of common induced genes by *H felis* and human gastric adenocarcinoma expression clusters. *IDO1*, B-cell markers (*IgJ*, *CD79a*, and *Pou2af1*), and the NK cell marker (*NKG7*) are highlighted in *blue font*. For mouse, the heatmap represents the fold increase in gene expression in male and female mice from 6-month *H felis*–infected stomachs compared to uninfected sex-matched stomach controls. For human, the heatmap represents the fold increase in median gene expression in a cluster compared to the median expression in the other clusters. The gene list was chosen to represent those that were overexpressed in both the 6-month *H felis*–infected mouse stomachs and in each of the 4 TCGA expression clusters (fold change $>$1.5) (The Cancer Genome Atlas Research, 2014). Genes are listed in order of highest to lowest fold change in human. (*B*) *Pie-chart* representation of the percentage of homologous human genes, for each expression cluster, that are induced in mice with a 6-month *H felis*–infected stomach. (*C*) *Pie-chart* representation of the percentage of induced homologous mouse genes that are induced in each human gastric adenocarcinoma expression cluster.

A

Human (*expression clusters*) **vs H^+/K^+-IFN-γ**

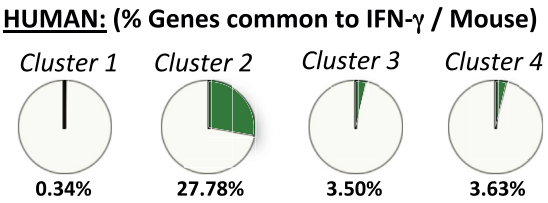

B

Human (*overall subtypes*) **vs *H. felis* model**

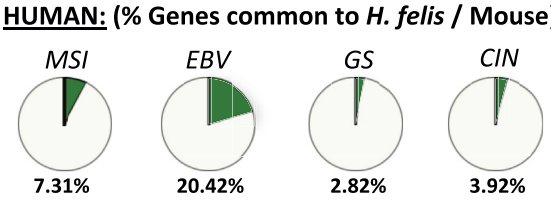

C

Human (*overall subtypes*) **vs H^+/K^+-IFN-γ**

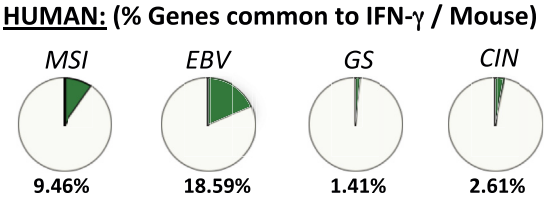

Supplementary Figure 14. Percentage similarity of genes induced in mouse gastric pre-neoplasia relative to homologous-induced human genes stratified by expression cluster or molecular subtype. (*A*) *Pie-chart* representation of induced mouse genes in the IFN-gamma–overexpression model relative to each human cluster. (*B*) *Pie-chart* representation of induced mouse genes in the *H felis* model relative to each human molecular subtype. (*C*) *Pie-chart* representation of induced mouse genes in the IFN-gamma–overexpression model relative to each human molecular subtype.